Successful arrest of photoreceptor and vision loss expands the therapeutic window of retinal gene therapy to later stages of disease

William A. Beltran[a,1,2], Artur V. Cideciyan[b,1,2], Simone Iwabe[a], Malgorzata Swider[b], Mychajlo S. Kosyk[b], Kendra McDaid[a], Inna Martynyuk[a], Gui-Shuang Ying[b], James Shaffer[b], Wen-Tao Deng[c], Sanford L. Boye[c], Alfred S. Lewin[d], William W. Hauswirth[c], Samuel G. Jacobson[b], and Gustavo D. Aguirre[a,2]

[a]Section of Ophthalmology, School of Veterinary Medicine, University of Pennsylvania, Philadelphia, PA 19104; [b]Scheie Eye Institute, Department of Ophthalmology, University of Pennsylvania Perelman School of Medicine, Philadelphia, PA 19104; [c]Department of Ophthalmology, University of Florida, Gainesville, FL 32610; and [d]Department of Molecular Genetics and Microbiology, University of Florida, Gainesville, FL 32610

Edited by Eric A. Pierce, Massachusetts Eye and Ear Infirmary, Boston, MA, and accepted by the Editorial Board September 10, 2015 (received for review May 20, 2015)

Inherited retinal degenerations cause progressive loss of photoreceptor neurons with eventual blindness. Corrective or neuroprotective gene therapies under development could be delivered at a predegeneration stage to prevent the onset of disease, as well as at intermediate-degeneration stages to slow the rate of progression. Most preclinical gene therapy successes to date have been as predegeneration interventions. In many animal models, as well as in human studies, to date, retinal gene therapy administered well after the onset of degeneration was not able to modify the rate of progression even when successfully reversing dysfunction. We evaluated consequences of gene therapy delivered at intermediate stages of disease in a canine model of X-linked retinitis pigmentosa (XLRP) caused by a mutation in the Retinitis Pigmentosa GTPase Regulator (*RPGR*) gene. Spatiotemporal natural history of disease was defined and therapeutic dose selected based on predegeneration results. Then interventions were timed at earlier and later phases of intermediate-stage disease, and photoreceptor degeneration monitored with noninvasive imaging, electrophysiological function, and visual behavior for more than 2 y. All parameters showed substantial and significant arrest of the progressive time course of disease with treatment, which resulted in long-term improved retinal function and visual behavior compared with control eyes. Histology confirmed that the human *RPGR* transgene was stably expressed in photoreceptors and associated with improved structural preservation of rods, cones, and ON bipolar cells together with correction of opsin mislocalization. These findings in a clinically relevant large animal model demonstrate the long-term efficacy of *RPGR* gene augmentation and substantially broaden the therapeutic window for intervention in patients with *RPGR*-XLRP.

retinal degeneration | gene therapy | late stage | XLRP | RPGR

The prevalence of neurodegenerative disorders worldwide has been projected to continue to rise dramatically. This situation is particularly true in developed countries that have seen an increase in the aging population coupled with a decline in common fatal conditions, such as stroke and heart attack (1). Chronic and debilitating neurodegenerative diseases impose a huge emotional, medical, and economical burden on patients, caregivers, and society (2, 3). Thus, treating neurodegenerations is one of the greatest scientific challenges taken up with the launch of the Brain Research through Advancing Innovative Neurotechnologies (BRAIN) Initiative in the United States and the Human Brain Project in Europe.

Decades of research have increased our knowledge of the pathogenic mechanisms of neurodegenerative diseases and led to the identification of potential molecular targets (4); however, the considerable resources invested in the development of new treatments have achieved only limited success (5). The lack of efficacy in clinical trials of novel therapies for Alzheimer's disease (6), Parkinson's disease (7), and amyotrophic lateral sclerosis (8) that appeared promising in preclinical studies has led to questions regarding the predictive validity of currently used animal models (9). Failures can result either because the experimental model does not recapitulate the human disease or because therapies are developed in animal models treated successfully at predegeneration stages as opposed to the intermediate- and advanced-degeneration stages found in most patients enrolled in clinical trials (Fig. 1*A*).

The retina, with its remarkable layered organization of interconnected neurons and its accessibility to imaging and functional studies, offers a "window" to the CNS (10). Novel insights into neurodegenerative processes have originated from the study of specific blinding ocular conditions such as glaucoma, age-related macular degeneration, and various inherited retinal degenerations, which include retinitis pigmentosa (RP). RP is a group of diseases that typically cause progressive degeneration of rod and cone photoreceptor cells and result in blindness. Over the last decades, preclinical evidence supporting the initiation of clinical trials of corrective gene therapy for RP has been based on successful proof of concept studies in which therapies were delivered before degeneration (11) or in models without a degenerative

Significance

Corrective gene therapies for inherited retinal degenerations are being developed with the expectation that even patients in later stages of the disease will benefit from such intervention. Evidence in animal models for a rescue after the onset of photoreceptor loss is scarce, and recent results from patients enrolled in two of the gene therapy clinical trials for a congenital form of blindness (RPE65-LCA) show that, despite transient improvement in visual function, photoreceptor cell death remains unabated. Here we show in a canine model for a common and severe form of X-linked retinal degeneration that gene therapy successfully stops photoreceptor cell death, improves the structure of retinal cells, and prevents vision loss for more than 2 y.

Author contributions: W.A.B., A.V.C., W.-T.D., W.W.H., S.G.J., and G.D.A. designed research; W.A.B., A.V.C., S.I., K.M., I.M., W.-T.D., and S.L.B. performed research; W.A.B., A.V.C., S.I., M.S., M.S.K., K.M., G.-S.Y., J.S., W.-T.D., S.L.B., A.S.L., W.W.H., S.G.J., and G.D.A. analyzed data; and W.A.B., A.V.C., A.S.L., W.W.H., S.G.J., and G.D.A. wrote the paper.

Conflict of interest statement: W.A.B., A.V.C., W.-T.D., S.L.B., A.S.L., W.W.H., S.G.J., and G.D.A. are inventors on the following patent application: PCT/US2013/022628. W.W.H. and the University of Florida have a financial interest in the use of adeno-associated virus therapies and own equity in a company (AGTC Inc.) that might, in the future, commercialize some aspects of this work.

This article is a PNAS Direct Submission. E.A.P. is a guest editor invited by the Editorial Board.

[1]W.A.B. and A.V.C. contributed equally to this work.

[2]To whom correspondence may be addressed. Email: wbeltran@vet.upenn.edu, cideciya@mail.med.upenn.edu, or gda@vet.upenn.edu.

This article contains supporting information online at www.pnas.org/lookup/suppl/doi:10.1073/pnas.1509914112/-/DCSupplemental.

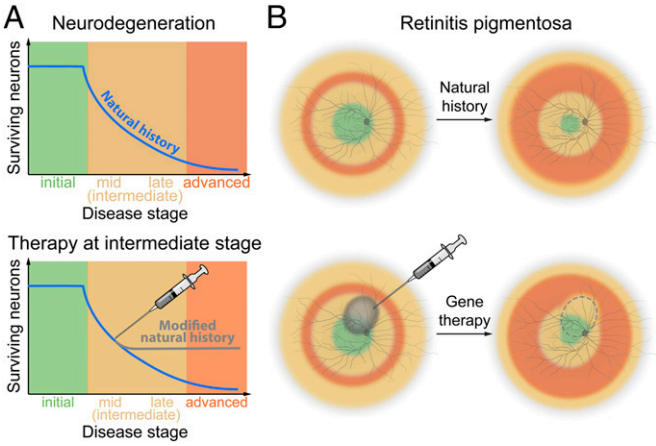

Fig. 1. Schematic of neurodegenerations and complex spatiotemporal interactions of potential treatments that seek to prevent disease or positively modify the natural history in retinitis pigmentosa. (*A*) Natural history of neuron death can be approximated as a delayed exponential function (*Upper*). Therapies initiated at intermediate stages aim to stop further neuron loss and rescue function (*Lower*). (*B*) In retinitis pigmentosa and allied diseases, there is a complex spatial distribution of photoreceptor degeneration. Typically an annulus is affected first, and over decades, the width of the annulus grows both centrifugally and centripetally (*Upper*). Subretinal gene therapy injections aim to modify the natural history locally by either preventing or arresting neurodegeneration depending on the local disease stage (*Lower*).

component (12–15). These experimental conditions fail to recapitulate the cellular and molecular environment of diseased photoreceptors in patients who have a complex spatial distribution of stages of disease across the retina (Fig. 1*B*). Considering the current evidence showing the difficulty to stop retinal degeneration (16, 17), it is of paramount importance to assess the efficacy of new therapies in more advanced disease stages.

X-linked RP caused by mutation in the Retinitis Pigmentosa GTPase Regulator (*RPGR*) gene is one of the most common inherited retinal degenerations (18–20). There are currently more than 300 distinct mutations (rpgr.hgu.mrc.ac.uk/supplementary/) identified in *RPGR*, and the majority are found in a glutamic acid-rich domain within exon ORF15 (21, 22). The natural course of *RPGR*-XLRP disease is severe, with males showing loss of night vision in the first decade of life (23). The disease onset in the naturally occurring or *Rpgr* KO mouse models is very late (23–25) as it corresponds to 35 human years (26), whereas the disease onset in two naturally occurring canine models of *RPGR*-XLRP (27–29) are earlier and correspond better to the human disease time course. Gene augmentation delivered by means of an adeno-associated viral (AAV) vector has been shown to be efficient in both the dog and mouse models (30, 31). Here we focused on using gene therapy to treat the intermediate disease stage of *RPGR*-XLRP in a canine model, at a time when ∼40% (mid stage) to 60% (late stage) of the neurons have already been lost to degeneration. We demonstrate efficacy in arresting further neurodegeneration with reversal of the photoreceptor disease, and retention of vision, lasting for more than 2 y. These results augur well for potential clinical treatment trials involving *RPGR*-XLRP patients who have substantial retinal degeneration but still retain some photoreceptors and suggest there is validity in treating and evaluating animals with mid-/late-course disease in other neurodegenerative disorders.

Results

Spatiotemporal Progression of Retinal Degeneration in Vivo. Mutations in the *RPGR* gene cause a severe and early-onset form of progressive retinal degeneration in humans and dogs (30). Of the two naturally occurring canine diseases, XLPRA2 is caused by a two-nucleotide deletion within ORF15 that results in a frameshift and truncation of the terminal 161 amino acid residues. Histologically, the outer (photoreceptor) nuclear layer (ONL) has a normal thickness (∼10–11 rows of nuclei) at 5 wk of age that corresponds to the age of onset of degeneration (29). The rate of photoreceptor neuronal death initially accelerates with a peak at ∼7 wk of age before returning to a reduced, yet constant, rate thereafter (29). The result is a rapid ONL thinning that leads to a thickness of approximately three rows of nuclei (∼30% of normal) (32) by ∼40 wk of age (29). In preparation for gene therapy strategies aimed at positively altering the natural history of the retinal degeneration, we first used in vivo imaging methods to evaluate the spatial distribution and temporal progression of ONL thickness changes with age. WT dogs show an ONL thickness distribution that peaks in the superior-central retina (Fig. 2*A*, *Left*) except for the small highly cone enriched fovea-like area (33) (Fig. S1 *A* and *B*). ONL thickness in XLPRA2 dogs can progress from near-normal at 8 wk to severe retina-wide thinning at 95 wk (Fig. S1*C*). Measurements at superior, supero-nasal, and inferior retinal locations show a regular and predictable pattern of ONL thinning with progression rates of −0.33 $\log_{10}$/y for superior and supero-nasal retinal regions and −0.45 $\log_{10}$/y for inferior retinal regions. These invariant log-linear periods of progression last to ∼78 wk of age. Thereafter, a slowing of the progression rate is apparent with an increase in measurement variability associated with severely thinned ONL (Fig. S1 *D* and *E*), reaching the axial resolution limit of the imaging system.

Dose–Response Function for Subretinal Gene Therapy. Subretinal gene therapy at initial stages of XLPRA2 disease, before detectable ONL thinning, can arrest the progressive retinal degeneration (30); however, the dose–response function of the treatment efficacy is not known. To determine the minimum effective titer (MET), we injected eight eyes at the onset of degeneration (5 wk of age) with over a 2.5 $\log_{10}$ range of titers, and used as a principal outcome measure ONL thickness maps recorded at 32–38 wk. Representative ONL maps show retention of thickness corresponding to the injection bleb for the two highest titers compared with lack of such effect for the lowest titer (Fig. 2*A*). Quantitative analysis of all eight eyes of five animals (Table S1) showed that the regions injected with a vector titer of 1.51×10^{11} vg/mL had an ONL thickness closest to WT (Fig. 2*B*). Injection volumes at 5 wk of age were 70 μL, which is a total vector dose of 10.6×10^9 vg. Lower titers resulted in ONL thickness expected from the untreated XLPRA2 natural history, and a higher titer did not reach the WT thickness, although it did show an effect of treatment (Fig. 2*B*). Thus, we consider the titer of 1.51×10^{11} vg/mL as the MET to a first approximation. Transgene expression was specifically detected by immunohistochemistry on retinal sections using an antibody (Table S2) that recognizes human but not canine RPGR protein. Immunolabeling was found exclusively in the bleb area, and semiquantitative assessment showed that the level of expression of the stable hRPGR variant was dose dependent. At the highest titers, the transgene was found throughout the length of the photoreceptors (with the exception of the outer segments; Fig. 2*C*) as previously reported when using retinal tissues fixed in paraformaldehyde for >1 h (30, 31). Immunolabeling of the RPGR transgene product has been shown to be restricted to the connecting cilium only when using a modified short (1–2 min) paraformaldehyde fixation protocol (31, 34). Importantly, control injections ($n = 7$) performed with balanced salt solution (BSS) in XLPRA2 eyes at different ages resulted in no measurable deviation of ONL thickness from the expected natural history (Fig. S1 *D* and *E*).

To determine whether there was toxicity of the vector to the retina, adult-size WT canine eyes were injected over a 2 $\log_{10}$ range of titers (Fig. S2), with a higher volume (150 μL) to cover a similar retinal area as achieved with 70 μL at 5 wk of age. For the MET and lower titer, the bleb region in WT eyes did not show a detectable difference from the surrounding uninjected region in

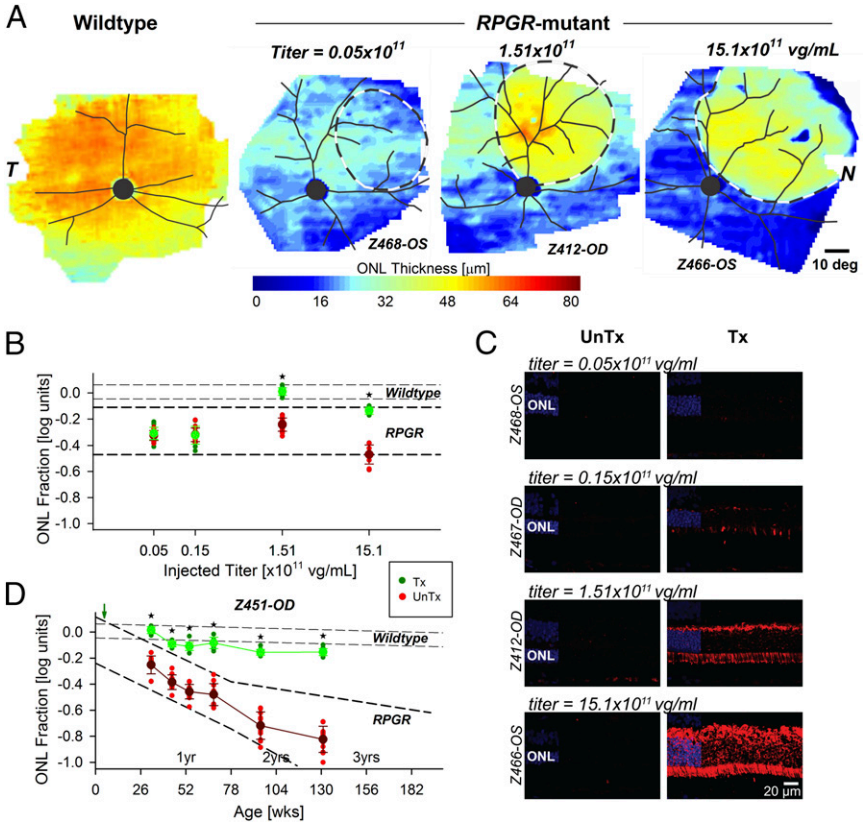

Fig. 2. Dose–response function and long-term durability of gene therapy intervention at initial disease stage. (*A*) Pseudocolor maps of mean ONL thickness topography in wild-type dogs ($n = 5$; ages 7–43 wk; mean = 25 wk) compared with individual eyes of representative XLPRA2 dogs (at 36–38 wk) subretinally treated at 5 wk of age in the supero-nasal quadrant with 70 μL of different vector titers. Dashed outline, the retinal region corresponding to the subretinal bleb. All eyes shown as equivalent right eyes and optic nerve and major blood vessels overlaid for ease of comparison. T, temporal; N, nasal retina. (*B*) ONL thickness fraction of WT ($\log_{10}$ units) at 36–38 wk of age as a function of vector titer injected at 5 wk. Data from treated (Tx, green) and untreated (UnTx, red) retinal regions are contrasted. The ranges of ONL fraction expected in WT eyes (thin dashed) or in untreated XLPRA2 eyes at 38 wk of age (thick dashed) are shown. In *B* and *D*, smaller symbols represent the individual data and larger symbols with error bars represent mean ± SD; $^*P < 0.01$ for paired *t* tests. (*C*) Immunolabeling of stable human RPGR transgene product on retinal sections at 43 wk of age (38 wk after treatment) is found exclusively in the photoreceptors at the bleb/treated areas and is dose dependent. (*D*) Serial ONL thickness measures between 32 and 131 wk of age after a superior subretinal vector injection at 5 wk of age (green arrow) to evaluate long-term durability with the 1.51×10^{11} vg/mL titer. Treated loci (green) remain near WT thickness (thin dashed lines), whereas untreated loci (red) show progressive thinning along the trajectory expected from the natural history of disease (thick dashed lines). Z468-OS and similar labels designate the individual animal and eye.

terms of ONL thickness. At the highest titer, however, there was evidence of mild ONL thickening at and around the bleb region in WT retinas (Fig. S2 *A* and *B*). Histology was not available, and mild toxicity of WT retinas to the vector at the titer of 15.1×10^{11} vg/mL cannot be ruled out; the significance of this finding to the mutant eyes is currently not clear. Taking all of the XLPRA2 and WT results into consideration, the remaining experiments were performed with the 1.51×10^{11} vg/mL titer of the AAV2/5 vector carrying a stable *hRPGR* transgene under the control of the hIRBP promoter.

Intervention at Initial Disease Stage Arrests Photoreceptor Loss and Rescues Vision for 3+ Y. Long-term durability of the therapeutic effect of intervention at the time that degeneration begins was evaluated next. An XLPRA2 retina was injected with MET at 5 wk of age, and ONL thickness across a wide extent of retina was mapped serially between 32 and 131 wk (Fig. 2*D*). Even at the first time point (27 wk after treatment), ONL thickness within the treated region was significantly thicker than the surrounding untreated region. Over the next 2 y, the untreated region lost ONL thickness along the trajectory consistent with the expected natural history of degeneration, whereas the injected region stably retained ONL thickness close to WT values (Fig. 2*D*). The difference in ONL thicknesses between the treated region and the surrounding untreated region progressively increased with time. Retinal function with full-field electroretinography (ERG) showed in the treated eye retention of rod and cone function up to the latest test date at 157 wk of age (Fig. S3*A*, *Left*). In the contralateral BSS-injected eye, rod function was not detectable and cone function was severely reduced. Visual function was assessed in an obstacle-avoidance course at 130–164 wk of age. Significantly improved navigation performance (shorter transit time and reduced number of collisions) under scotopic and low mesopic ambient illumination (≤0.2 lx) was observed when testing the treated eye in comparison with the untreated eye; treated eye results were within the range observed with WT dogs (Fig. S3*B*, *Left*).

Gene Therapy Intervention at Mid-Stage Disease Arrests Photoreceptor Loss and Rescues Vision for Up to 3 Y. The stability of rescue following intervention at mid-stage disease was evaluated next. XLPRA2 retinas were injected with MET at 12 wk of age (volume injected: 150 μL; dose: 22.7×10^9 vg), after the peak of photoreceptor cell death that results in a loss of ~40% of the ONL (29). ONL thickness across a wide extent of retina was mapped serially between 31 and 131 wk (Fig. 3 *A* and *B*). Although ONL maps at the first time point (31 wk of age, 19 wk after treatment) suggested some rescue in the treated region, this was more evident at later time points (Fig. 3*A* and Fig. S4*A*). In three treated XLPRA2 dogs, both in the superior and inferior retina, measurements of

ONL thickness on each side of the treatment border showed an initial decline that followed the natural course of disease, but ONL loss in the treated region was halted at 31 wk of age. The rescue persisted up to 131 wk of age, the latest evaluation point.

Histological assessment in an XLPRA2 dog at 113 wk of age confirmed the in vivo imaging results with a clear demarcation in ONL thickness at the border of the bleb (Fig. 3*C*). There was a substantially thicker ONL in the treated (approximately seven rows of nuclei) vs. untreated (approximately one to three rows of nuclei) regions. Inner (IS) and outer (OS) segments of photoreceptors had a normal appearance within the treated area, but they were almost completely lost in the untreated region (Fig. 3*D*).

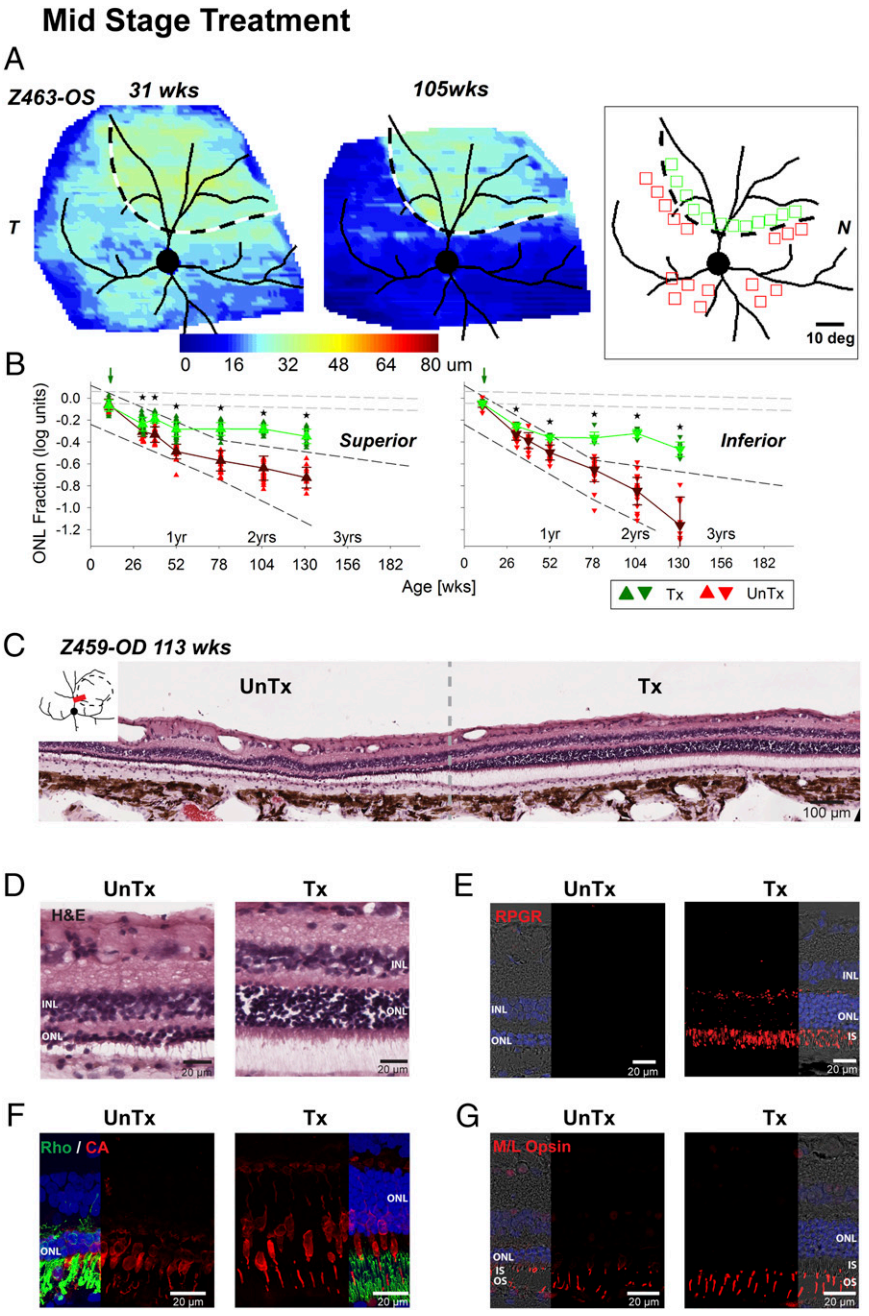

Fig. 3. Efficacy and long-term stability of gene therapy intervention at mid-stage disease. (*A*) Pseudocolor maps of ONL thickness topography at 31 and 105 wk of age in an XLPRA2 dog treated at 12 wk of age. Dashed outline, the retinal region corresponding to the subretinal vector bleb at treatment. Schematic, right, paired loci across the treatment boundary and in the inferior retina chosen for quantitative evaluation. Eyes are shown as equivalent right eyes with optic nerve and major blood vessels overlaid for ease of comparability. T, temporal; N, nasal retina. (*B*) Progressive changes in ONL fraction recorded serially between 11 and 130 wk of age in treated (green) and untreated (red) loci in the superior (*Left*) and inferior (*Right*) retinas of three XLPRA2 dogs. Vertical green arrows depict the timing of treatment at 12 wk of age. Dashed lines show the range of ONL fraction expected in WT eyes or natural history of progression in untreated XLPRA2 eyes. Smaller symbols represent the individual data and larger symbols with error bars represent mean ± SD; $*P < 0.01$ for paired *t* tests between treated and untreated loci. (*C–G*) Retinal morphology at 113 wk of age in the untreated (*Left*) and treated (*Right*) areas of an XLPRA2 dog injected at 12 wk. (*C*) H&E-stained section across the treatment boundary (red bar in diagram shows section location). (*D*) H&E stain, higher magnification view. (*E*) IHC labeling of stable human RPGR transgene product. (*F*) Cone arrestin (CA, red) and rhodopsin (RHO, green) double IHC. (*G*) R/G opsin (red) IHC labeling. Z463-OS and similar labels designate the individual animal and eye.

Expression of the stable human RPGR transgene product was localized exclusively to photoreceptors of the treated area (Fig. 3*E*) and was found throughout the cell except in the OS (30). Immunolabeling with cone arrestin and rod and cone opsin antibodies confirmed the structural rescue of both photoreceptor populations (Fig. 3*F*), as well as the reversal of opsin mislocalization (Fig. 3 *F* and *G*) in the treated area. Not only was cone structure better preserved, but counts of total (M/L and S) cones showed a higher number of cells in the treated relative to untreated areas, and approximately twice as many S cones were found to express S opsin in their OS (Fig. S5 *A* and *B*). To determine the effect of *RPGR* augmentation on the structure of the photoreceptor sensory cilium, three ciliary markers (rootletin, centrin-3, and acetylated α-tubulin) were used for IHC. Their pattern of labeling in the treated area was normal (Fig. S5*C*) and similar to that seen in an untreated XLPRA2 at the injection age of 12 wk (Fig. S6 *A* and *B*), but very different from the reduced immunostaining in the untreated area at 113 wk (Fig. S5*C*). Thus, mutant retina treated by *RPGR* augmentation retained molecular components of the sensory cilium to their normal site and levels of expression. Overall, these results suggest that intervention at mid-stage disease is able to stop cell death. Based on the observation that rod and cone IS and OS structure in treated 113-wk-old animal (Fig. 3 *C* and *D*) is more normal than at the 12 wk of age, the injection time point (Fig. S6*B*; H&E), there appears to be preliminary evidence that treatment could actually reverse structural alterations in the surviving photoreceptors. Further support comes from restoration of normal dendritic arborization of ON bipolar cells located within the treated area (Fig. S5*D*). In the treated eyes of two dogs, ERG showed retained rod and cone function up to the latest test date at 157 wk of age (Fig. S3*A*, *Center*). Visually guided behavior in an obstacle avoidance course was also significantly improved under scotopic and mesopic illumination when testing the treated eyes between 130 and 164 wk of age (Fig. S3*B*, *Right*).

Efficacy and Durability for Up to 2+ Y of Gene Therapy Intervention at Late-Stage Disease. To assess whether the window for therapeutic intervention could be extended to a more advanced disease stage, XLPRA2 retinas were injected with MET at 26 wk of age. At this age, the ONL is approximately four to five rows of nuclei thick in the central/midperipheral retina (~40–50% of normal), and the structure of the OS is severely compromised (29). Topographic maps of ONL thickness from early postinjection time points did not indicate a rescue effect for up to 40 wk (Fig. 4*A* and Fig. S4*B*). By 52 wk of age, a region of rescue became qualitatively visible and statistically significant (Fig. 4*B*). From that time point up to 131 wk of age, ONL loss was halted in the treated area of the superior retina, but continued unabated in the untreated region (Fig. 4 *A* and *B* and Fig. S4*B*). This rescue was confirmed histologically in an XLPRA2 dog at 113 wk of age. The ONL was thicker in the treated (approximately four rows of nuclei) than in the untreated (approximately one to two rows of nuclei) region, and photoreceptors retained the normal elongated IS and OS (Fig. 4 *C* and *D*). Expression of the stable human RPGR transgene in the treated areas (Fig. 4*E*) was associated with better preserved rod and cone OS structure and with correction of rod opsin mislocalization (Fig. 4 *F* and *G*). An increase in the number of all cones (M/L + S), as well as S cones with preserved OS, was found in the treated vs. untreated area (Fig. 5 *A* and *B*). The immunolabeling pattern of the photoreceptor sensory cilium was also better preserved in the treated area at 113 wk of age (Fig. 5*C*) and resembled that seen in an untreated dog at 24 wk of age (Fig. S6*C*). The presence of inner retinal gliosis was assessed by GFAP immunolabeling and did not reveal any increased reactivity of astrocytes or Müller cells in either the treated or untreated areas. Finally, rod bipolar cells reestablished the dendritic arborizations that were absent at the 26-wk injection time point (29), and had completely retracted in the untreated regions at 113 wk of age (Fig. 5*D*). ERG analysis performed at 105 wk of age showed preserved rod function in all three dogs and cone function in two of three animals as illustrated for dog Z465 (Fig. 6*A*). Although in the third dog (Z464) similar amplitudes of persistent cone function were recorded from both the treated and untreated eye, combined analysis of the ERG data from all three dogs showed a statistically significant positive rescue of rod-mediated retinal function (Fig. 6*B*). The mean ERG values at 105 wk of age from the three treated dogs were compared with that of seven WT adult dogs and showed that rod-mediated b-wave amplitude was 8% of WT, and mixed rod-cone a- and b-wave amplitudes were, respectively, 6% and 11% of WT. Because at 26 wk of age the XLPRA2 retina has lost 50–60% of its photoreceptors (primarily rods) and only ~1/5 of the retina was treated, these values suggest that maximal achievable ERG preservation was obtained from the treated area. ERG measurements repeated at 157 wk of age (latest test date) in the two remaining XLPRA2 dogs showed persistent rescue of both rod and cone function in the treated eyes (Fig. S3*A*, *Right*). Combined analysis of the performance of these two dogs in an obstacle-avoidance course between 130 and 164 wk of age showed a faster transit time (within the range of WT dogs) and reduced number of collisions when testing the treated vs. the untreated eyes under scotopic and mesopic ambient illumination. Visual function was further investigated in these animals between 149 and 162 wk of age by assessing their ability to detect a dim blue flashing light in a forced two-choice Y maze (Fig. S7). An improved ability to detect the light stimulus was seen when testing the treated eyes. Combined analysis of the data collected from both dogs during all eight sessions showed a statistically significant difference in the success rate of the treated vs. untreated eye (91% vs. 63%; $P < 0.001$; Fig. 6*D*).

Discussion

Inherited retinopathies are Mendelian diseases caused by thousands of mutations in >200 distinct genes (18). Most commonly, there is a progressive loss of vision due to neurodegeneration of retinal photoreceptors, and there is no cure or treatment (35). Potential therapeutic approaches can be categorized into three groups: (*i*) prevention of degeneration before it starts, (*ii*) slowing the rate of progression, and (*iii*) replacement of lost photoreceptors and their intraretinal connectivity (35). In the current work, we used an AAV2/5 vector to intervene with gene augmentation therapy both early and late in a naturally occurring canine model of *RPGR*-XLRP and demonstrated long-lasting arrest of retinal degeneration, restoration of normal structure in the remaining photoreceptors and bipolar cells, and rescue of vision.

Defining the Natural History of Disease as a Prelude to Interventions at Different Stages. In human clinical trials to date, AAV-vectored gene therapy for the *RPE65* form of Leber congenital amaurosis (LCA) has shown improvement of some aspects of vision (36, 37), but there is recent evidence in patients from two of the ongoing trials that such intervention has not been able to stem the progression rate of retinal degeneration (16, 38, 39). In naturally occurring canine models, both of *RPE65*-LCA and others, gene therapy has produced similar results: intervention after the onset of photoreceptor degeneration has not been able to modify the natural history of the disease (16) or to restore visual function unless adjunctive treatments are done (40). When the intervention preceded major loss of photoreceptors, prevention of retinal degeneration has often been achieved (16, 30, 41, 42) but not always (17).

In mice, there is an extensive literature on gene augmentation therapy showing improved photoreceptor survival as long as the intervention is applied before or at very early stages of retinal degeneration (43–47). Other work has shown positive effects of gene therapy when applied to disorganized retinas with rosettes (48). Successful rescue of photoreceptors with gene augmentation has been difficult to achieve when applied late in the disease natural

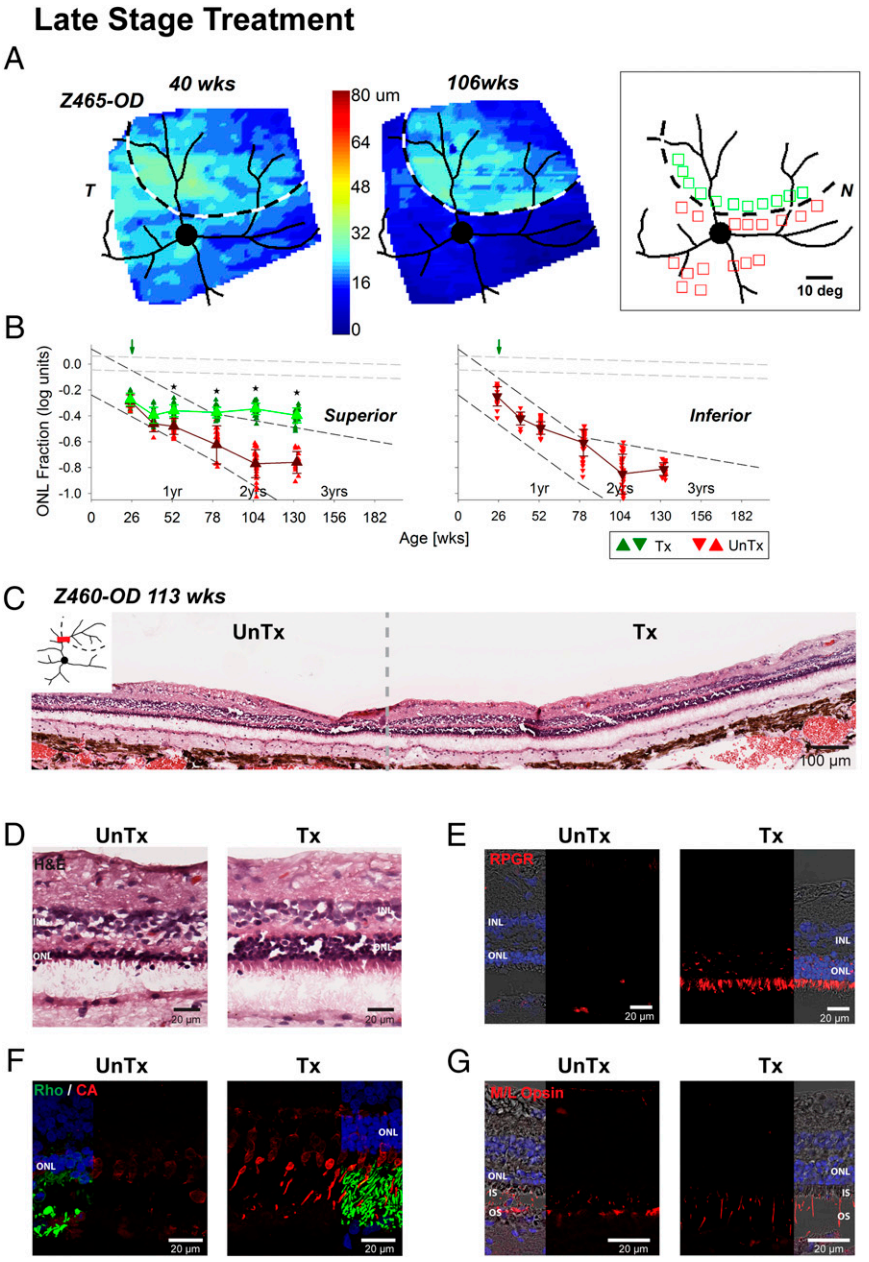

Fig. 4. Efficacy and long-term durability of gene therapy intervention at late-stage disease. (*A*) Pseudocolor maps of ONL thickness topography at 40 and 106 wk of age in an XLPRA2 dog treated at 26 wk of age. Dashed outline, the retinal region corresponding to the subretinal vector bleb at treatment. Schematic, right, paired loci across the treatment boundary and in the inferior retina chosen for quantitative evaluation. Eyes are shown as equivalent right eyes with optic nerve and major blood vessels overlaid for ease of comparability. T, temporal; N, nasal retina. (*B*) Progressive changes in ONL fraction recorded serially between 25 and 130 wk of age in treated (green) and untreated (red) loci in the superior retina (*Left*). None of the three treated eyes received injection in the inferior retina; thus, only untreated loci are shown in inferior retina (*Right*). Vertical green arrows depict the timing of treatment at 26 wk of age. Dashed lines show the range of ONL fraction expected in WT eyes or natural history of progression in untreated XLPRA2 eyes. Smaller symbols represent the individual data and larger symbols with error bars represent mean ± SD; $*P < 0.01$ for paired *t* tests between treated and untreated loci. (*C–G*) Retinal morphology at 113 wk of age in the untreated (*Left*) and treated (*Right*) areas of an XLPRA2 dog injected at 26 wk. (*C*) H&E-stained section across the treatment boundary (red bar in diagram shows section location). (*D*) H&E stain, higher magnification view. (*E*) IHC labeling of stable human RPGR transgene product. (*F*) Cone arrestin (CA, red) and rhodopsin (RHO, green) double IHC. (*G*) R/G opsin (red) IHC labeling. Z465-OD and similar labels designate the individual animal and eye.

history. There have been reports of success (31, 49, 50) but with the caveat of a lack of quantitative definition of spatiotemporal natural history of retinal degeneration at the time of the intervention.

It is well known that human retinopathies demonstrate very complex spatiotemporal patterns of disease progression (Fig. 1*B*) (51, 52), even though underlying genetic mutations are presumed to be expressed in all retinal cells of relevance. In mouse models, and their localized treatments with gene therapy, spatiotemporal gradients of natural disease progression are not often investigated. However, when carefully examined, there can be major gradients of ONL thickness that significantly varies within and between retinas (23). Therefore, we first quantitatively defined the spatiotemporal natural history of retinal degeneration in the XLPRA2 dogs (Fig. S1). Both in the superior and inferior retina loci, exponential functions (16) with different parameters described the progressive loss of photoreceptors for the first 1.5 y of life. Extrapolating the

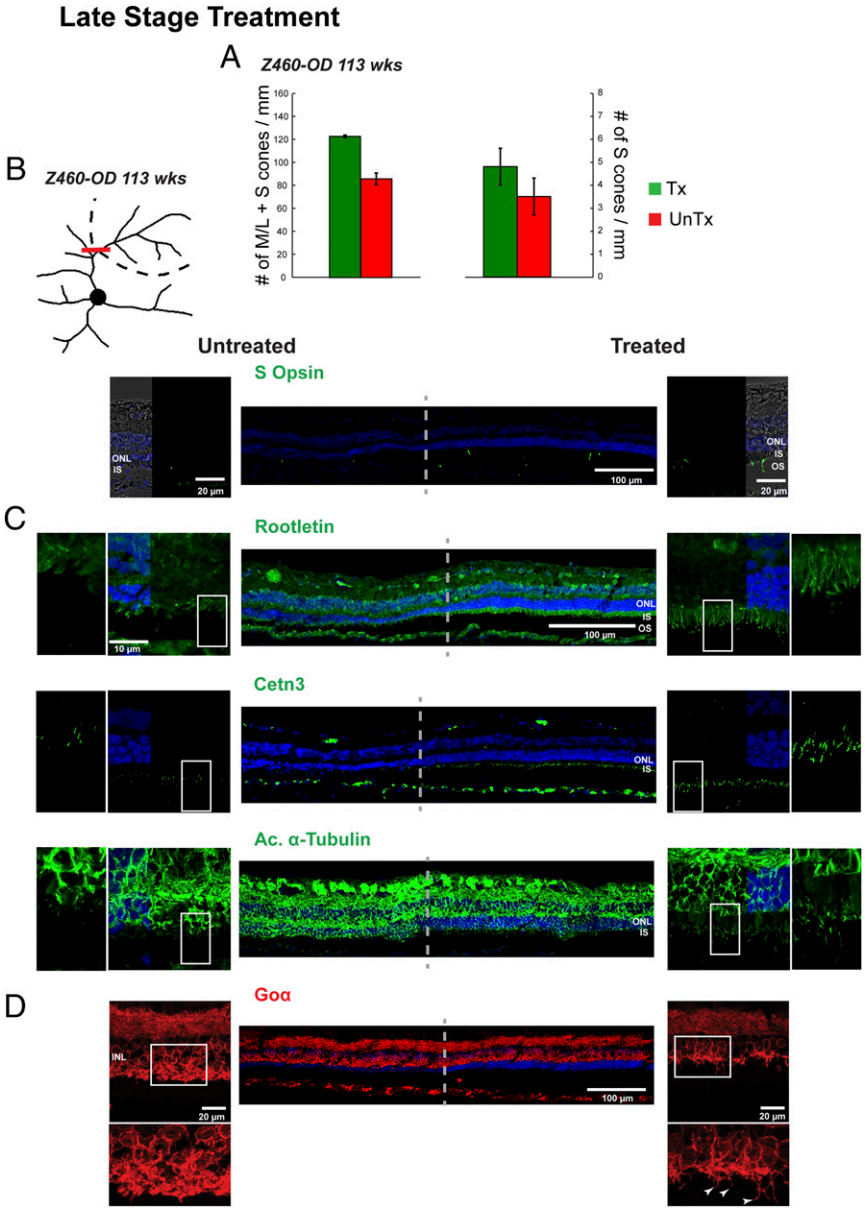

Fig. 5. Structural rescue of photoreceptors and bipolar cells in a XLPRA2 dog treated at late-stage disease. Histology at 113 wk of dog Z460 injected at 26 wk of age. (*A*) Mean (±SD) number of (M/L + S) and S cones per millimeter of retina length in the treated and untreated areas ($n = 4$). (*B*) S cone opsin (green) IHC labeling in the untreated area (*Left*), across the treatment boundary (*Center*), and in the treated area (*Right*). The schematic drawing illustrates the treatment area (dashed black curve), and the location of the section showing the treatment boundary (red line). (*C*) IHC labeling of the sensory cilium of photoreceptors with rootletin, centrin-3 (Cetn3), and acetylated α-tubulin antibodies. (*D*) Goα IHC labeling of ON-bipolar cells. White arrowheads point to their dendrites.

natural history to young ages implied an initial delay of degeneration that likely ranged from 5 to 12 wk of life and varied by location and animal. The rate of degeneration was slower in the superior and supero-nasal retina (–0.33 $\log_{10}$/y) compared with the inferior retina (–0.45 $\log_{10}$/y).

Comparability of Progression of Disease in the Canine and Human. In patients with *RPGR*-XLRP, the exact spatiotemporal natural history of retinal degeneration is not known: this lack of knowledge extends to all other molecular forms of RP. There are, however, published estimates of rates of vision loss in *RPGR*-XLRP, and these can be used to estimate underlying retinal degeneration. For example, ERG amplitudes have been shown to change by −0.07 $\log_{10}$/y for cones and rods (53). These full-field averaged values are in the same order of magnitude as psychophysical sensitivity changes rates reported for cone vision ranging from −0.06 to −0.09 $\log_{10}$/y at specific extramacular retinal locations (54). Previous work has shown that rod and cone losses tend to be equal in this condition (55). Under the simplifying assumptions of a delayed exponential progression of disease (56) and a relationship between the square of ONL thickness and light sensitivity (57), the rate of ONL thickness change in human *RPGR*-XLRP can be estimated to fall in the range of −0.03 to −0.05 $\log_{10}$/y. Using allometric scaling based on maximum lifespan (26), the human progression estimate corresponds to −0.18 to −0.31 $\log_{10}$ per canine-equivalent years, which is similar to the rate of −0.33 $\log_{10}$/y estimated in the superior retina of XLPRA2 dogs but slower than the −0.45 $\log_{10}$/y estimated in the inferior retina. Thus, the current studies were performed to place the treatment injections in the superior retinal locations whenever possible. Future studies of human *RPGR*-XLRP should ideally include direct measurement of the thickness of the photoreceptor layer and its progressive thinning as we previously performed in *RPE65*-LCA (16) to provide a quantitative and predictive spatiotemporal measure of the natural history of degeneration in advance of upcoming treatment trials.

The Window of Opportunity for *RPGR* Gene Augmentation Can Be Expanded to Later Stages of Retinal Degeneration. After demonstrating the long-term (>3 y) stable rescue effect provided by early gene therapy intervention, we focused our efforts on determining

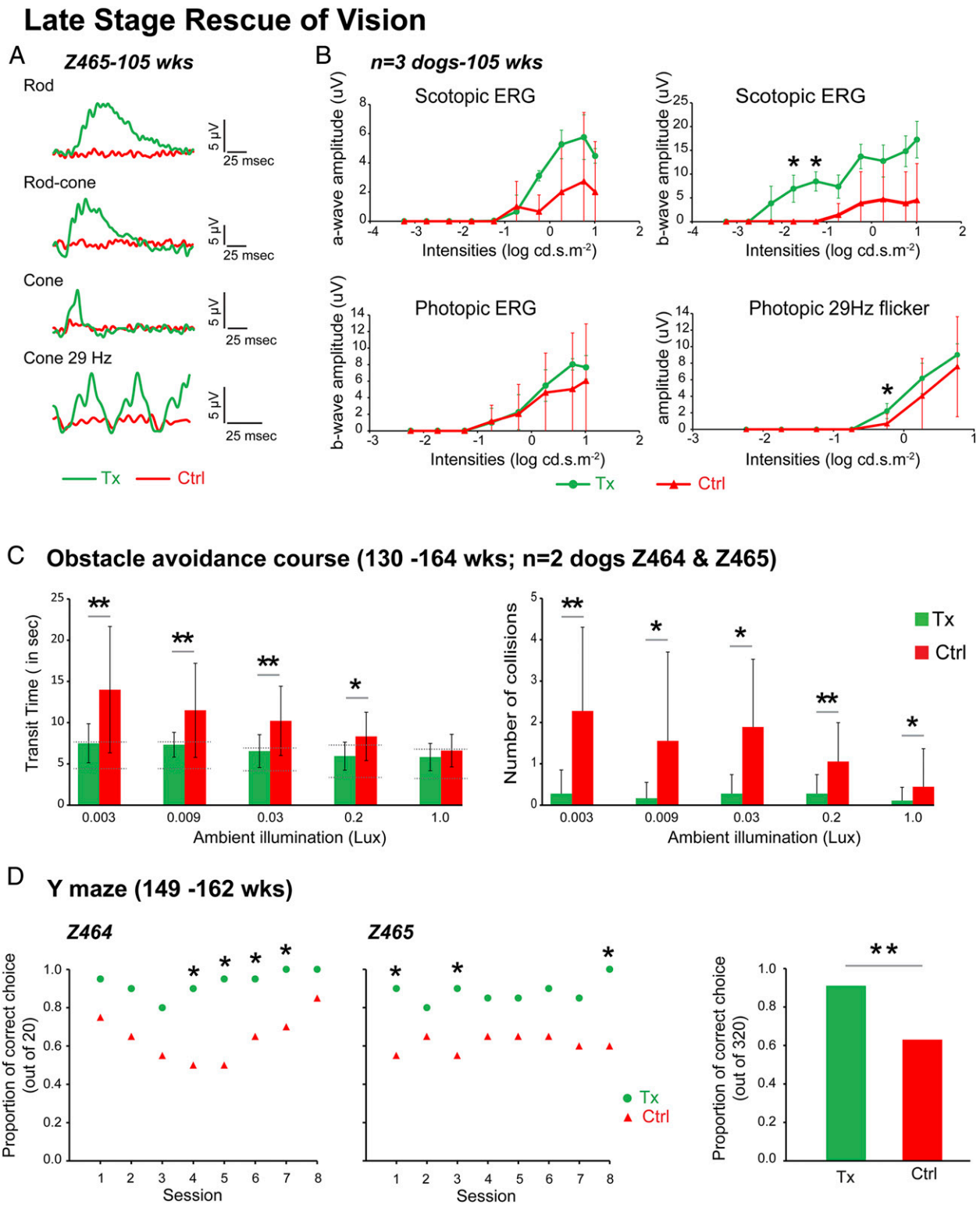

Fig. 6. Long-term durability of retinal function and visual behavior after gene therapy intervention at late-stage disease. (*A*) Representative ERG traces of rod (−1.74 log cd·s·m^{-2}), mixed rod-cone (1.01 log cd·s·m^{-2}) recorded dark adapted, and cone (1.01 log cd·s·m^{-2}) responses to single stimuli or 29-Hz cone flicker (0.76 log cd·s·m^{-2}) recorded light adapted at 105 wk of age in an XLPRA2 dog treated at 26 wk of age. (*B*) Summary of all rod and cone ERG results recorded at 105 wk of age from three XLPRA2 dogs treated at late-stage disease. (*C*) Mean (±SD) transit time and mean (±SD) number of collisions in an obstacle-avoidance course under different ambient light intensities. The treated vs. control eyes of two XLPRA2 dogs (Z464 and Z465) injected at 26 wk of age were compared after pooling data recorded during nine trials conducted between 130 and 164 wk of age. Gray dotted lines represent the 95% CI of the transit time of WT dogs ($n = 3$). No collisions were observed with these WT dogs. (*D*) Visually guided behavior in a forced two-choice Y maze of the same two XLPRA2 dogs treated at 26 wk of age. (*Left* and *Center*) Performance of each dog when assessing the treated vs. the control eye during eight test sessions conducted between 149 and 162 wk of age. (*Right*) Visual performance of the treated vs. control eyes after pooling together data from both dogs and from all eight sessions (total of 320 trials). *$P < 0.05$, **$P < 0.001$ from paired Student *t* test (for ERG data) and from generalized linear model testing (for obstacle course and Y maze data) between treated and control eyes.

whether *RPGR* gene augmentation could arrest the natural course of disease when delivered at patient-relevant stages of retinal degeneration. For this, XLPRA2 dogs at mid- and late-stage disease were subretinally injected with the same viral titer (1.51×10^{11} vg/mL) as used at the initial stage (this study and ref. 30). Because the numbers of photoreceptors are reduced by ~50–60% at 26 wk of age (late-stage intervention), the titer used would be predicted to result in an approximately twofold higher vector load per photoreceptor cell compared with dogs treated at 5 wk of age with their full photoreceptor complement (initial-stage intervention). No signs of ocular toxicity were detected clinically or histologically even when treating XLPRA2 with a 10-fold higher viral titer (15.1×10^{11} vg/mL) than that selected for the long-term studies. This lack of toxicity suggests that the AAV construct used may have a reasonably high therapeutic index. These results contrast, however, with the findings from another group that observed both short- and long-term toxicity in the *Rpgr* KO mouse when using a different AAV serotype/promoter/*RPGR* transgene at doses, respectively, 3- and 10-fold higher than the one that provided the most potent therapeutic effect (31).

Following intervention at mid and late stages of disease, there was a latency of up to 26 wk before the rate of ONL loss was substantially altered. Such a "delay" in ONL rescue could be explained by a lower efficiency of the vector at transducing older/diseased photoreceptors or the inability for corrective gene therapy to modify the fate of cells that are already irreversibly damaged and committed to cell death. After ONL loss was halted, the rescue effect was shown to be stable for more than 2 y following intervention at late-stage disease. Histological assessment in two dogs treated at mid and late stage confirmed the morphological rescue of both rods and cones, correction of opsin mislocalization, and reversal of the early dendritic retraction of bipolar cells (29). The structural preservation of surviving photoreceptors including their sensory cilium, and the positive remodeling of the inner retina was associated with improved ERG amplitudes of rods, cones, and postreceptoral neurons in all treated eyes. Significantly, we now demonstrate for the first time to our knowledge that *RPGR* gene augmentation prolongs rod-driven visual behavior, an observation that could not be made at earlier time points when significant vision under scotopic illumination still persisted in the control eyes (30).

Improving the Predictive Value of Animal Models Used to Test Treatments for Retinal Degeneration. Over the last decades, several therapeutic strategies that include the use of neuroprotective agents, antiapoptotic factors, immunotherapy, and corrective gene therapy have been developed with the ultimate goal of preventing or halting photoreceptor degeneration. With few exceptions (31, 49, 50), preclinical evidence gathered to support the initiation of clinical trials has been based on proof-of-concept studies conducted in animal models at a predegenerative stage (11, 58–61). A limitation is that these experiments at predegenerate stages fail to recapitulate the cellular and molecular environment of surviving photoreceptors in patients with advanced disease. So does drug development for retinal degenerative diseases run a risk of high attrition as seen with the therapy pipelines for Alzheimer and Parkinson's diseases (6, 7)? Disappointing results with sustained delivery of the neuroprotective agent ciliary neurotrophic factor (CNTF) for the treatment of early- and late-stage RP in two studies (62) and evidence that patients involved in two of the gene therapy clinical trials for the *RPE65* form of Leber congenital amaurosis (LCA) show unabated photoreceptor and vision loss despite initial visual improvement (16, 38, 39) suggest that evidence in animal models for long-term efficacy and testing at clinically relevant stages of disease are needed to improve the predictive value of preclinical studies.

In conclusion, although regulatory agencies such as the US Food and Drug Administration, which are responsible for approving investigations of new drugs in humans, require preclinical data from animal pharmacology and toxicology studies, there has been a poor "return on investment" of many drug trials for neurodegenerative diseases. This situation calls for reconsidering the importance of establishing proof of concept in animal models that truly recapitulate the stages of disease of patients to be enrolled in phase II/III clinical trials. Despite the increased financial pressure that this would exercise on both academia and industry, this appears to be a necessary step to increase the success rate in translating new drugs to the clinical phase. For retinal gene therapy approaches, this would involve confirming efficient transduction of targeted cells in an animal that models the various human stages of degeneration and positive alteration of the natural course of disease before filing an Investigational New Drug application. Our successful late-stage intervention and long-term follow-up results in a clinically relevant large animal model now provide the necessary proof of concept to support a clinical trial for *RPGR*-XLRP.

Materials and Methods

All dogs were bred and maintained at the University of Pennsylvania Retinal Disease Studies Facility (RDSF). The studies were carried out in strict accordance with the recommendations in the *Guide for the Care and Use of Laboratory Animals* of the National Institutes of Health (63) and the USDA's Animal Welfare Act and Animal Welfare Regulations and complied with the ARVO Statement for the Use of Animals in Ophthalmic and Vision Research. The protocols were approved by the Institutional Animal Care and Use Committee of the University of Pennsylvania. *RPGR* mutant (XLPRA2) (28, 29) and WT dogs were used to characterize the natural course of ONL thinning as a function of age (16) and the response to subretinal injections with an AAV2/5 vector (64) carrying a stabilized human $RPGR^{1\text{-}ORF15}$ cDNA under the control of a human IRBP promoter (30, 65). The stabilized human $RPGR^{1\text{-}ORF15}$ cDNA (stable hRPGR) contained seven in-frame deletions, one 3-bp insertion, and 65-bp substitutions spread throughout the AG-rich region of exon ORF15 compared with the published (GenBank: NM_001034853) human $RPGR^{1\text{-}ORF15}$ sequence (34). Stable hRPGR was the same sequence as used in our previous *RPGR* gene augmentation study in XLPRA1 and XLPRA2 dogs (30). Assessment of the response to *RPGR* gene transfer was made by means of clinical ophthalmic examinations, en face and cross-sectional in vivo retinal imaging (Fig. S8), electroretinography, visual behavior testing that included the use of an obstacle-avoidance course and a forced 2-choice Y maze, and morphological evaluation on retinal histological section (16, 29, 30, 61). Methodological details are provided in *SI Materials and Methods*.

ACKNOWLEDGMENTS. We thank Dr. Cheryl Craft (University of Southern California) and Dr. Uwe Wolfrum (University of Mainz) for providing, respectively, the cone arrestin and centrin3 antibodies; and the Retinal Disease Studies Facility staff, Dr. J. M. Guzman, J. Andrews-Labenski, F. Letterio, M. Suplick, M. Leonard, and L. Melnyk for technical and research coordination support. This work was supported by National Institutes of Health Grants R24EY-022012, 2PNEY-018241, RO1EY-017549, RO1EY-06855, RO1EY-013203, P30EY-001583, and P40-OD010939. Work was also funded by the Foundation Fighting Blindness, the Macula Vision Research Foundation, Hope for Vision, and the Van Sloun fund for canine genetic research.

1. Hebert LE, Weuve J, Scherr PA, Evans DA (2013) Alzheimer disease in the United States (2010-2050) estimated using the 2010 census. *Neurology* 80(19):1778–1783.
2. Wimo A, Prince M (2010) *World Alzheimer Report 2010 The Global Ecomomic Impact of Dementia - Executive summary* (Alzheimer's Disease International, London), pp 1–9.
3. Olesen J, Gustavsson A, Svensson M, Wittchen HU, Jönsson B; CDBE2010 study group; European Brain Council (2012) The economic cost of brain disorders in Europe. *Eur J Neurol* 19(1):155–162.
4. Ribe EM, Serrano-Saiz E, Akpan N, Troy CM (2008) Mechanisms of neuronal death in disease: Defining the models and the players. *Biochem J* 415(2):165–182.
5. Li C, Ebrahimi A, Schluesener H (2013) Drug pipeline in neurodegeneration based on transgenic mice models of Alzheimer's disease. *Ageing Res Rev* 12(1):116–140.
6. Cummings JL, Morstorf T, Zhong K (2014) Alzheimer's disease drug-development pipeline: Few candidates, frequent failures. *Alzheimers Res Ther* 6(4):37.
7. Bartus RT, Weinberg MS, Samulski RJ (2014) Parkinson's disease gene therapy: Success by design meets failure by efficacy. *Mol Ther* 22(3):487–497.

8. Gordon PH, et al.; Western ALS Study Group (2007) Efficacy of minocycline in patients with amyotrophic lateral sclerosis: A phase III randomised trial. *Lancet Neurol* 6(12):1045–1053.
9. Sabbagh JJ, Kinney JW, Cummings JL (2013) Animal systems in the development of treatments for Alzheimer's disease: Challenges, methods, and implications. *Neurobiol Aging* 34(1):169–183.
10. London A, Benhar I, Schwartz M (2013) The retina as a window to the brain-from eye research to CNS disorders. *Nat Rev Neurol* 9(1):44–53.
11. Acland GM, et al. (2001) Gene therapy restores vision in a canine model of childhood blindness. *Nat Genet* 28(1):92–95.
12. Kong J, et al. (2008) Correction of the disease phenotype in the mouse model of Stargardt disease by lentiviral gene therapy. *Gene Ther* 15(19):1311–1320.
13. Colella P, et al. (2013) Myosin7a deficiency results in reduced retinal activity which is improved by gene therapy. *PLoS One* 8(8):e72027.
14. Tolmachova T, et al. (2012) CHM/REP1 cDNA delivery by lentiviral vectors provides functional expression of the transgene in the retinal pigment epithelium of choroideremia mice. *J Gene Med* 14(3):158–168.
15. Tolmachova T, et al. (2013) Functional expression of Rab escort protein 1 following AAV2-mediated gene delivery in the retina of choroideremia mice and human cells ex vivo. *J Mol Med (Berl)* 91(7):825–837.
16. Cideciyan AV, et al. (2013) Human retinal gene therapy for Leber congenital amaurosis shows advancing retinal degeneration despite enduring visual improvement. *Proc Natl Acad Sci USA* 110(6):E517–E525.
17. Lhériteau E, et al. (2014) Successful gene therapy in the RPGRIP1-deficient dog: A large model of cone-rod dystrophy. *Mol Ther* 22(2):265–277.
18. Bramall AN, Wright AF, Jacobson SG, McInnes RR (2010) The genomic, biochemical, and cellular responses of the retina in inherited photoreceptor degenerations and prospects for the treatment of these disorders. *Annu Rev Neurosci* 33:441–472.
19. Wright AF, Chakarova CF, Abd El-Aziz MM, Bhattacharya SS (2010) Photoreceptor degeneration: Genetic and mechanistic dissection of a complex trait. *Nat Rev Genet* 11(4):273–284.
20. Branham K, et al. (2012) Mutations in RPGR and RP2 account for 15% of males with simplex retinal degenerative disease. *Invest Ophthalmol Vis Sci* 53(13):8232–8237.
21. Vervoort R, et al. (2000) Mutational hot spot within a new RPGR exon in X-linked retinitis pigmentosa. *Nat Genet* 25(4):462–466.
22. Shu X, et al. (2007) RPGR mutation analysis and disease: An update. *Hum Mutat* 28(4): 322–328.
23. Huang WC, et al. (2012) RPGR-associated retinal degeneration in human X-linked RP and a murine model. *Invest Ophthalmol Vis Sci* 53(9):5594–5608.
24. Hong DH, et al. (2000) A retinitis pigmentosa GTPase regulator (RPGR)-deficient mouse model for X-linked retinitis pigmentosa (RP3). *Proc Natl Acad Sci USA* 97(7): 3649–3654.
25. Thompson DA, et al. (2012) Rd9 is a naturally occurring mouse model of a common form of retinitis pigmentosa caused by mutations in RPGR-ORF15. *PLoS One* 7(5):e35865.
26. Wright AF, et al. (2004) Lifespan and mitochondrial control of neurodegeneration. *Nat Genet* 36(11):1153–1158.
27. Zeiss CJ, Acland GM, Aguirre GD (1999) Retinal pathology of canine X-linked progressive retinal atrophy, the locus homologue of RP3. *Invest Ophthalmol Vis Sci* 40(13):3292–3304.
28. Zhang Q, et al. (2002) Different RPGR exon ORF15 mutations in Canids provide insights into photoreceptor cell degeneration. *Hum Mol Genet* 11(9):993–1003.
29. Beltran WA, Hammond P, Acland GM, Aguirre GD (2006) A frameshift mutation in *RPGR* exon ORF15 causes photoreceptor degeneration and inner retina remodeling in a model of X-linked retinitis pigmentosa. *Invest Ophthalmol Vis Sci* 47(4):1669–1681.
30. Beltran WA, et al. (2012) Gene therapy rescues photoreceptor blindness in dogs and paves the way for treating human X-linked retinitis pigmentosa. *Proc Natl Acad Sci USA* 109(6):2132–2137.
31. Wu Z, et al. (2015) A long-term efficacy study of gene replacement therapy for RPGR-associated retinal degeneration. *Hum Mol Genet* 24(14):3956–3970.
32. Aguirre G, O'Brien P (1986) Morphological and biochemical studies of canine progressive rod-cone degeneration. 3H-fucose autoradiography. *Invest Ophthalmol Vis Sci* 27(5):635–655.
33. Beltran WA, et al. (2014) Canine retina has a primate fovea-like bouquet of cone photoreceptors which is affected by inherited macular degenerations. *PLoS One* 9(3): e90390.
34. Deng WT, et al. (2015) Stability and Safety of an AAV Vector for treating RPGR-ORF15 X-linked Retinitis Pigmentosa. *Hum Gene Ther* 26(9):593–602.
35. Jacobson SG, Cideciyan AV (2010) Treatment possibilities for retinitis pigmentosa. *N Engl J Med* 363(17):1669–1671.
36. Cideciyan AV (2010) Leber congenital amaurosis due to RPE65 mutations and its treatment with gene therapy. *Prog Retin Eye Res* 29(5):398–427.
37. Jacobson SG, et al. (2012) Gene therapy for leber congenital amaurosis caused by RPE65 mutations: Safety and efficacy in 15 children and adults followed up to 3 years. *Arch Ophthalmol* 130(1):9–24.
38. Jacobson SG, et al. (2015) Improvement and decline in vision with gene therapy in childhood blindness. *N Engl J Med* 372(20):1920–1926.
39. Bainbridge JW, et al. (2015) Long-term effect of gene therapy on Leber's congenital amaurosis. *N Engl J Med* 372(20):1887–1897.
40. Komáromy AM, et al. (2013) Transient photoreceptor deconstruction by CNTF enhances rAAV-mediated cone functional rescue in late stage CNGB3-achromatopsia. *Mol Ther* 21(6):1131–1141.
41. Narfström K, et al. (2008) Morphological aspects related to long-term functional improvement of the retina in the 4 years following rAAV-mediated gene transfer in the RPE65 null mutation dog. *Adv Exp Med Biol* 613:139–146.
42. Petit L, et al. (2012) Restoration of vision in the pde6β-deficient dog, a large animal model of rod-cone dystrophy. *Mol Ther* 20(11):2019–2030.
43. Pang JJ, et al. (2008) AAV-mediated gene therapy for retinal degeneration in the rd10 mouse containing a recessive PDEbeta mutation. *Invest Ophthalmol Vis Sci* 49(10): 4278–4283.
44. Tan MH, et al. (2009) Gene therapy for retinitis pigmentosa and Leber congenital amaurosis caused by defects in AIPL1: Effective rescue of mouse models of partial and complete Aipl1 deficiency using AAV2/2 and AAV2/8 vectors. *Hum Mol Genet* 18(12): 2099–2114.
45. Pawlyk BS, et al. (2010) Replacement gene therapy with a human RPGRIP1 sequence slows photoreceptor degeneration in a murine model of Leber congenital amaurosis. *Hum Gene Ther* 21(8):993–1004.
46. Koch S, et al. (2012) Gene therapy restores vision and delays degeneration in the CNGB1(-/-) mouse model of retinitis pigmentosa. *Hum Mol Genet* 21(20):4486–4496.
47. Wert KJ, Davis RJ, Sancho-Pelluz J, Nishina PM, Tsang SH (2013) Gene therapy provides long-term visual function in a pre-clinical model of retinitis pigmentosa. *Hum Mol Genet* 22(3):558–567.
48. Pellissier LP, et al. (2015) Gene therapy into photoreceptors and Müller glial cells restores retinal structure and function in CRB1 retinitis pigmentosa mouse models. *Hum Mol Genet* 24(11):3104–3118.
49. Simons DL, Boye SL, Hauswirth WW, Wu SM (2011) Gene therapy prevents photoreceptor death and preserves retinal function in a Bardet-Biedl syndrome mouse model. *Proc Natl Acad Sci USA* 108(15):6276–6281.
50. Wert KJ, Sancho-Pelluz J, Tsang SH (2014) Mid-stage intervention achieves similar efficacy as conventional early-stage treatment using gene therapy in a pre-clinical model of retinitis pigmentosa. *Hum Mol Genet* 23(2):514–523.
51. Cideciyan AV, et al. (1998) Disease sequence from mutant rhodopsin allele to rod and cone photoreceptor degeneration in man. *Proc Natl Acad Sci USA* 95(12):7103–7108.
52. Cideciyan AV, et al. (2009) ABCA4 disease progression and a proposed strategy for gene therapy. *Hum Mol Genet* 18(5):931–941.
53. Hoffman DR, et al. (2004) A randomized, placebo-controlled clinical trial of docosahexaenoic acid supplementation for X-linked retinitis pigmentosa. *Am J Ophthalmol* 137(4):704–718.
54. Birch DG, et al. (2015) Rates of decline in regions of the visual field defined by frequency-domain optical coherence tomography in patients with RPGR-mediated X-linked retinitis pigmentosa. *Ophthalmology* 122(4):833–839.
55. Jacobson SG, et al. (1997) Disease expression in X-linked retinitis pigmentosa caused by a putative null mutation in the RPGR gene. *Invest Ophthalmol Vis Sci* 38(10): 1983–1997.
56. Clarke G, et al. (2000) A one-hit model of cell death in inherited neuronal degenerations. *Nature* 406(6792):195–199.
57. Jacobson SG, et al. (2005) Identifying photoreceptors in blind eyes caused by RPE65 mutations: Prerequisite for human gene therapy success. *Proc Natl Acad Sci USA* 102(17):6177–6182.
58. Smith AJ, et al. (2003) AAV-Mediated gene transfer slows photoreceptor loss in the RCS rat model of retinitis pigmentosa. *Mol Ther* 8(2):188–195.
59. Min SH, et al. (2005) Prolonged recovery of retinal structure/function after gene therapy in an Rs1h-deficient mouse model of x-linked juvenile retinoschisis. *Mol Ther* 12(4):644–651.
60. Pang JJ, et al. (2006) Gene therapy restores vision-dependent behavior as well as retinal structure and function in a mouse model of RPE65 Leber congenital amaurosis. *Mol Ther* 13(3):565–572.
61. Komáromy AM, et al. (2010) Gene therapy rescues cone function in congenital achromatopsia. *Hum Mol Genet* 19(13):2581–2593.
62. Birch DG, Weleber RG, Duncan JL, Jaffe GJ, Tao W; Ciliary Neurotrophic Factor Retinitis Pigmentosa Study Groups (2013) Randomized trial of ciliary neurotrophic factor delivered by encapsulated cell intraocular implants for retinitis pigmentosa. *Am J Ophthalmol* 156(2):283–292.e1.
63. Committee on Care and Use of Laboratory Animals (1996) *Guide for the Care and Use of Laboratory Animals* (Natl Inst Health, Bethesda), DHHS Publ No (NIH) 85–23.
64. Beltran WA, et al. (2010) rAAV2/5 gene-targeting to rods:dose-dependent efficiency and complications associated with different promoters. *Gene Ther* 17(9):1162–1174.
65. al-Ubaidi MR, et al. (1992) Bilateral retinal and brain tumors in transgenic mice expressing simian virus 40 large T antigen under control of the human interphotoreceptor retinoid-binding protein promoter. *J Cell Biol* 119(6):1681–1687.
66. Allocca M, et al. (2007) Novel adeno-associated virus serotypes efficiently transduce murine photoreceptors. *J Virol* 81(20):11372–11380.
67. Mussolino C, et al. (2011) AAV-mediated photoreceptor transduction of the pig cone-enriched retina. *Gene Ther* 18(7):637–645.
68. Boye SE, et al. (2012) The human rhodopsin kinase promoter in an AAV5 vector confers rod- and cone-specific expression in the primate retina. *Hum Gene Ther* 23(10):1101–1115.
69. Komáromy AM, Varner SE, de Juan E, Acland GM, Aguirre GD (2006) Application of a new subretinal injection device in the dog. *Cell Transplant* 15(6):511–519.
70. Garcia MM, Ying GS, Cocores CA, Tanaka JC, Komáromy AM (2010) Evaluation of a behavioral method for objective vision testing and identification of achromatopsia in dogs. *Am J Vet Res* 71(1):97–102.
71. Zeger SL, Liang KY (1986) Longitudinal data analysis for discrete and continuous outcomes. *Biometrics* 42(1):121–130.

Supporting Information

Beltran et al. 10.1073/pnas.1509914112

SI Materials and Methods

Animals. All dogs were bred and maintained at the University of Pennsylvania Retinal Disease Studies Facility (RDSF). The studies were carried out in strict accordance with the recommendations in the Guide for the Care and Use of Laboratory Animals of the National Institutes of Health and the USDA's Animal Welfare Act and Animal Welfare Regulations and complied with the ARVO Statement for the Use of Animals in Ophthalmic and Vision Research. The protocols were approved by the Institutional Animal Care and Use Committee of the University of Pennsylvania. All electroretinographic and noninvasive imaging procedures, as well as subretinal injections, were performed under general anesthesia, as previously described (30, 61, 64). Ocular tissues were collected after euthanasia with i.v. injection of euthanasia solution (Euthasol; Virbac), and all efforts were made to improve animal welfare and minimize discomfort. Included were 21 eyes of 18 normal (WT) and 25 eyes of 14 XLPRA2 dogs (Table S1).

Vector Development and Stability of the Vector Sequence. AAV serotype 2/5 was chosen because murine, canine, porcine, and nonhuman primate (NHP) rods and/or cones are known to be transduced with this vector serotype (30, 64, 66–68). A 235-nt segment of the proximal human IRBP (hIRBP) promoter (65) was chosen to transduce canine rods and cones (30). The human *RPGR*$^{1\text{-}ORF15}$ cDNA was chosen as the transgene because it is an RPGR isoform enriched in photoreceptors. It is 3,449 bp in length, which allows more than 1,200 bp for the promoter, polyA addition sequence, and AAV ITRs. The transgene contains ORF15, the location of a major fraction of *RPGR*-XLRP mutations and a known hot spot for spontaneous mutations (21, 22). The high mutability of exon ORF15 may be related to a central repetitive, purine-rich region that may promote DNA polymerase arrest and slipped-strand mispairing during replication because the majority of disease causing mutations are out-of-frame deletions within these short repetitive regions (21). Consistent with this, cloning of the RPGR$^{1\text{-}ORF15}$ sequence into AAV vectors required screening of multiple colonies to identify a stable sequence that was found multiple times from individual bacterial colonies. Evidence for the stability of this human RPGR$^{1\text{-}ORF15}$ sequence (named "stable hRPGR") in vectors came from finding that the vector that was initially used to successfully treat *RPGR*-mutant dogs (30) contained the identical sequence as three more independently produced AAV vectors used in this study. Full details on the stable hRPGR sequence have been recently published (34).

Subretinal Injections. Subretinal injections of BSS or vector were performed under general anesthesia with a subretinal cannula as previously reported (30, 64, 69), and volumes injected (70–150 μL) were adjusted to the dogs' age/globe size aiming to produce a bleb that covered ∼1/5 of the retinal surface. The location of the subretinal bleb was recorded immediately after each injection.

Optical Coherence Tomography Imaging and Analyses. En face and retinal cross-sectional imaging was performed with the dogs under general anesthesia. Overlapping en face images of reflectivity with near-infrared illumination (820 nm) were obtained (Spectralis HRA+OCT) with 30° and 55° diameter lenses to delineate fundus features such as optic nerve, retinal blood vessels, boundaries of injection blebs, retinotomy sites, and other local changes. Custom programs (MatLab 7.5; The MathWorks) were used to digitally stitch individual photos into a retina-wide panorama. Spectral domain-optical coherence tomography (SD-OCT) was performed with linear and raster scans (Spectralis HRA+OCT). Overlapping 30° × 20° raster scans were recorded covering large regions of the retina (Fig. S8). Postacquisition processing of OCT data was performed with custom programs (MatLab 7.5; The MathWorks). For retina-wide topographic analysis, integrated backscatter intensity of each raster scan was used to locate its precise location and orientation relative to retinal features visible on the retina-wide mosaic formed by NIR reflectance images (Fig. S8). Individual longitudinal reflectivity profiles (LRPs) forming all registered raster scans were allotted to regularly spaced bins (1° × 1°) in a rectangular coordinate system centered at the optic nerve; LRPs in each bin were aligned and averaged. Intraretinal peaks and boundaries corresponding to the ONL were segmented using both intensity and slope information of backscatter signal along each LRP. For all topographic results, locations of blood vessels, optic nerve head, and bleb boundaries were overlaid for reference.

ERG Recording and Analyses. Dogs were premedicated with s.c. injections of atropine and acepromazine, and their pupils were dilated with atropine (1%), tropicamide (1%), and phenylephrine (10%). After induction with i.v. propofol, dogs were maintained under general inhalation anesthesia (isoflurane), and their pulse rate, oxygen saturation, and temperature were monitored for constancy during the entire procedure. Full-field flash electroretinography was performed on both eyes using a custom-built Ganzfeld dome fitted with the LED stimuli of a ColorDome stimulator (Diagnosys). After 20 min of dark adaptation, rod and mixed rod-cone–mediated responses (averaged four times) to single 4-ms white flash stimuli of increasing intensities (from −3.24 to 1.01 log cd·s·m^{-2}) were recorded. Following 5 min of white light adaptation (1.53 log cd·m^{-2}), cone-mediated signals (averaged 10 times) to a series of single flashes (from −2.24 to 1.01 log cd·s·m^{-2}) and to a 29.4-Hz flicker (averaged 20 times; from −2.24 to 0.76 log cd·s·m^{-2}) stimuli were recorded. Amplitudes of the a- and b-waves of the scotopic ERG, and the peak to peak amplitudes of the photopic single flash and 29.4-Hz flicker were measured. Mean and SD of these ERG parameters were calculated at 105 wk of age (n = 3 for both the mid- and late-stage treatment groups) and compared between treated and paired control eyes using a paired t test. All statistical analyses was performed using SAS v9.4 (SAS Institute), and two-sided $P < 0.05$ was considered statistically significant.

Retinal Morphology and Immunohistochemistry. At 113 wk of age, an XLPRA2 dog from each of the mid- and late-stage treatment groups was euthanized. Eyes were immediately enucleated, fixed in 4% paraformaldehyde (PFA) for 3 h followed by 2% PFA for up to 6 d, trimmed, and embedded in optimal cutting temperature media as previously reported (29, 30). Ten-micrometer-thick serial sections that encompassed the nontreated, the boundary, and the treated/bleb area were cut on a cryostat (Microm HM550; Thermo Fisher Scientific). Blood vessel landmarks identified by H&E staining were used to determine the precise location of the retinal cryosections on the vascular pattern of the en face cSLO images. Sequential sections were immunolabeled with primary antibodies and cell-specific markers (Table S2). Before incubation with the rootletin, centrin-3, and acetylated α-tubulin antibodies, heat-induced epitope retrieval was performed by

incubating the retinal sections in citrate buffer (pH = 6) at 125 °C for 10 min in a pressure cooker. The antigen–antibody complexes were visualized with fluorochrome-labeled secondary antibodies (Alexa Fluor, 1:200; Molecular Probes), and Hoechst 33342 counterstain (Molecular Probes, Thermo Fisher Scientific) was used to label cell nuclei. H&E-stained sections were examined by widefield microscopy (Axioplan; Carl Zeiss Meditec), and the images were digitally captured (Spot 4.0 camera; Diagnostic Instruments) and imported into a graphics program (Adobe Illustrator) for display. Sections labeled for fluorescent immunohistochemistry were examined by confocal microscopy (Leica TCS SP5; Leica Microsystems CMS GmbH), and digital images were taken, processed using the Leica Application suite program, and imported into a graphics program (Illustrator; Adobe). Total numbers of cell bodies from M/L and S cones labeled with human cone arrestin antibody and that of S opsin-positive OS were determined in both the treated and untreated areas on four retinal sections per eye that extended over the treatment boundary. Cell counts were expressed per millimeter of retinal length.

Visual Behavior Testing in an Obstacle-Avoidance Course. After a period of socialization and training, visually guided behavior was evaluated in a 3.6-m-long custom-built obstacle-avoidance course (70) that included five displaceable panels. Eyes were tested individually by placing an opaque ocular shield (Aestek; Oculoplastik) on the contralateral cornea. Both eyes were tested three times under each of five distinct ambient illuminations that ranged from scotopic (0.003, 0.009, and 0.03 lx) to mesopic (0.2 and 1 lx) conditions. These light intensities were calibrated with a light meter (IL1700; International Light Technologies) at the level of dog's eye. The position of the five panels was randomly changed between each of the three trials per eye per illumination. The contralateral eye was tested with the same set of panel positions. Random selection of the eye to be tested first was made before the session.

Dogs were first adapted for 20 min to the lowest ambient illumination (0.003 lx) before running through the course; subsequently, the room illumination was increased to the next level of brightness, and dogs were adapted for 10 min and tested as previously described. The session ended when testing under the five ambient illuminations was completed (total of 30 trials). Two digital cameras (Sony Handycam) located above the obstacle course recorded the navigation performance of the dogs. The infrared imaging function of the camera enabled recording under the dimmest light conditions. An experienced observer who was masked to the experimental design reviewed all of the videos to measure for each trial the transit time measured in seconds between the first forward motion at the entrance of the course and the moment the animal completely passed through the exit gate, and the total number of collisions into the walls or moveable obstacle panels. For each of the three groups (initial-, mid-, and late-stage degeneration), the data collected from all dogs on the 3 testing days (130, 146, and 164 wk) were combined. The mean difference in transit time and number of collisions under each ambient illumination between treated eyes and the contralateral control eyes, its 95% CI, and associated P value were calculated from generalized linear models using generalized estimating equations (GEEs) to account for the correlation among repeated measurements from the same animal (71). All statistical analyses were performed using SAS v9.4 (SAS Institute), and two-sided $P < 0.05$ was considered statistically significant.

Visual Behavior Testing in a Y Maze. A Y maze composed of a 1.78-m-long entry arm and two 1.27-m-long exit arms was built with black PVC (Fig. S7). The ceiling was made with a black opaque fabric, and two black strip curtains were placed at the exits, and a sliding black panel at the entry isolated the interior of the Y maze from any external light. A custom-made power supply controlled at each exit a horizontal 19-cm strip of six LEDs spaced every 3.81 cm (GSLEDIP12; Nemalux) that was used to emit a flickering (3 Hz) blue light (470 nm) stimulus (50-ms duration; Fig. S7). Each of these strips of LEDs was oriented toward the bifurcation of the Y maze, where it produced at dog's eyes level a corneal irradiance of $\sim 1 \times 10^{-6}$ mW/cm^2 (measured with an IL1700 illuminometer). Following a period of socialization during which bright sources of white light (6,500 K; stimulus: 3 Hz, 50-ms duration; corneal irradiance at bifurcation: 6.25 mW/cm^2) delivered by strips of six LEDs (Nemalux) were used to train the dogs at selecting the correct (illuminated) exit, the animals were tested under scotopic conditions with the significantly dimmer blue light stimuli. As with the obstacle avoidance course, each eye was tested separately by placing a black ocular shield on the contralateral eye. Random selection of the eye to be tested first was made before the session. After a dark adaptation period of 20 min, the dog was run in the Y maze 20 times for each eye. Only one strip of LEDs was randomly turned on for any given trial. Both the right and left light stimuli were selected 10 of 20 times. Once the dog had completed its 20 trials for one eye, the contralateral eye was subsequently tested. An infrared sensitive camera placed inside the Y maze recorded the choice of the dog when it entered the bifurcation. An experienced observer who was masked to the experimental design reviewed all of the videos and recorded for each eye the number of times (of 20 trials) that the dog correctly selected the illuminated exit. Comparison of the proportion of correct exit choices (of 20 trials) between the treated and untreated fellow eye of two XLPRA2 dogs treated at 26 wk of age (late-stage disease) was done for each of the eight testing sessions that were conducted between 130 and 164 wk of age. Comparison of correct exit choices (of 320 trials) was also done after combining data from both dogs and all eight sessions. The mean difference in the proportion of correct choice between the treated eye and fellow eye, its 95% CIs, and associated P value were calculated from generalized linear models using GEEs to account for the correlation among repeated measurements from the same animal (71). All statistical analyses were performed using SAS v9.4 (SAS Institute), and two-sided $P < 0.05$ was considered statistically significant.

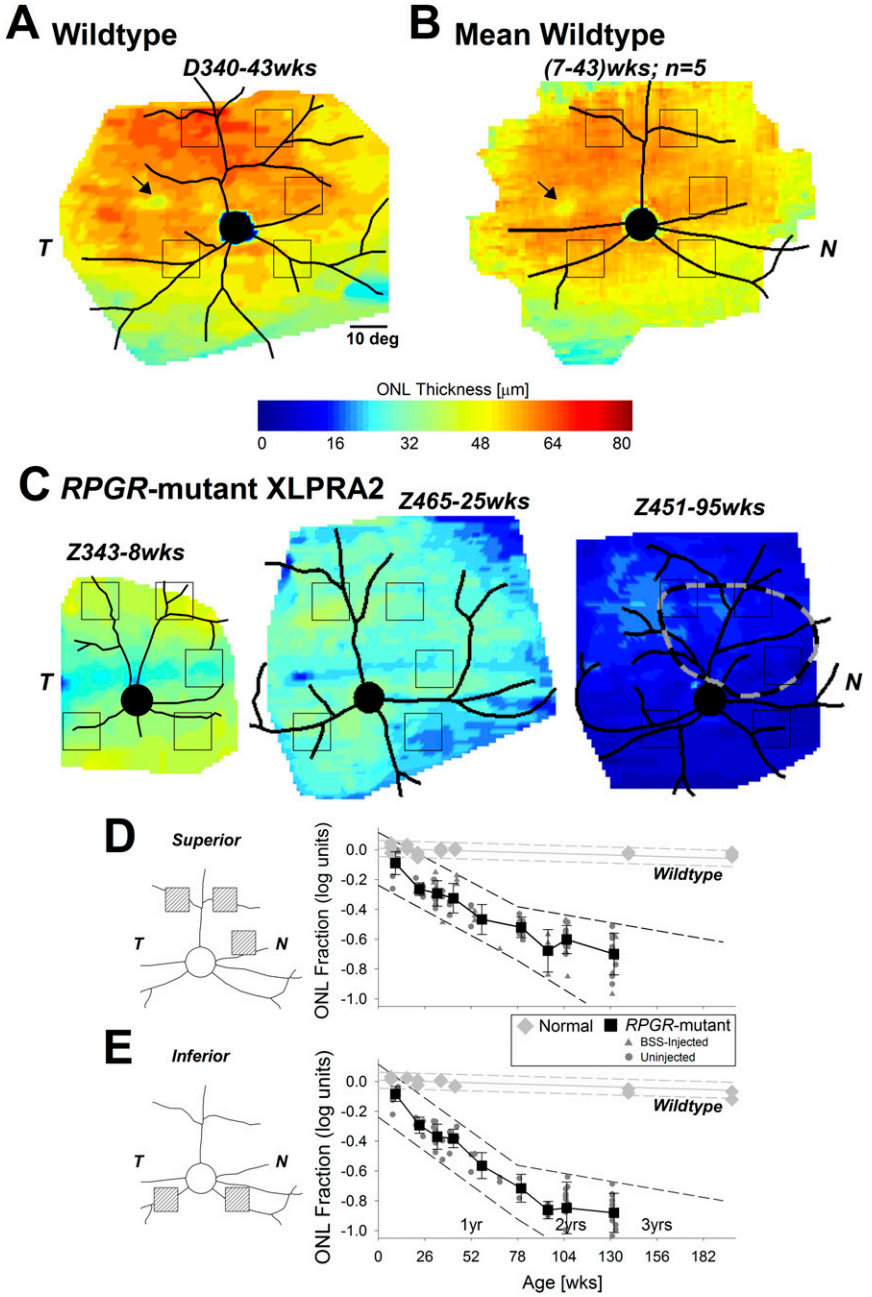

Fig. S1. Natural history of retinal degeneration in *RPGR*-mutant XLPRA2 dogs. (*A*) Pseudocolor maps of ONL thickness topography in a representative young WT dog. Black squares demarcate the five standard locations used for analysis. (*B*) The mean value of the ONL thickness in young WT dogs ($n = 5$; ages 7–43 wk; mean = 25 wk) after each map has been translated and rotated to bring the centers of the optic nerves and the locations of the canine fovea-like region (black arrowheads) into congruence. This panel is repeated from Fig. 2*A* for the convenience of the readers. (*C*) Representative ONL thickness topographies in *RPGR*-mutant XLPRA2 dogs at different ages show its progressive thinning with age. Also shown (*Right*) is a representative control eye at 95 wk of age that was injected subretinally with BSS at 5 wk; dashed lines demarcate the BSS bleb; three superior standard locations fall within the BSS bleb and two inferior locations fall outside. There is no obvious treatment effect or toxicity resulting from the BSS injection. T, temporal; N, nasal retina. (*D* and *E*) The natural history of ONL thickness within three standard locations in superior and supero-nasal retina (*D*) and two standard locations in the inferior retina (*E*) in WT (light gray symbols) and XLPRA2 eyes (dark gray symbols). Note, data from two older WT dogs are shown for reference but not included in the mean normal calculation. The main XLPRA2 natural history data originates from nine untreated control eyes of seven dogs (ages 8–146 wk; mean = 31 wk). There were additional data from eight eyes with subretinal BSS injections. At each standard location, ONL thickness was divided by the mean WT ONL at the corresponding location to produce ONL fraction, and the logarithm (to the base 10) was calculated. Log ONL fractions are plotted as a function of age for the three superior and supero-nasal retinal loci (*D*) and two inferior retinal loci (*E*). Parallel dashed lines (up to 78 wk) demarcate the 95% prediction intervals. Estimates of the underlying exponential progression rates are −0.33 $\log_{10}$/y for the superior retina loci and −0.45 $\log_{10}$/y for the inferior retina loci. After 78 wk, there is an apparent slowing of rate of degeneration and greater variability. Smaller symbols represent the individual data and larger symbols with error bars represent mean ± SD.

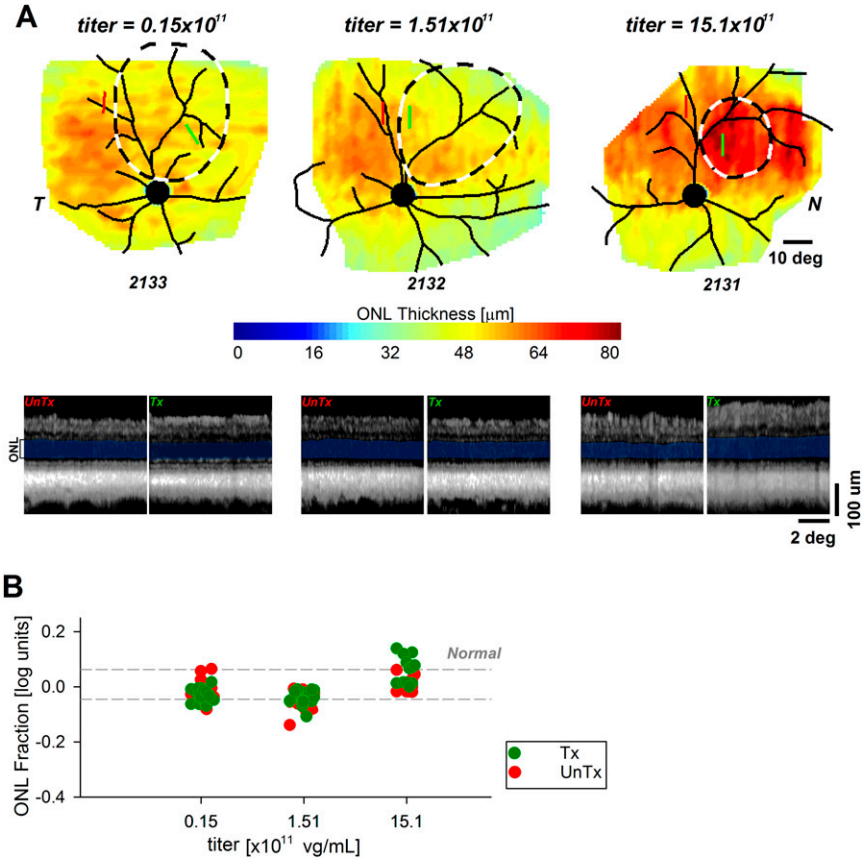

Fig. S2. WT eyes injected with increasing titers of vector. (*A*) Pseudocolor maps of ONL thickness topography at 34 wk of age in representative WT eyes each injected at 24 wk with 150 μL of a different viral vector titer. Dashed outline, the retinal region corresponding to the subretinal bleb. Red and green lines, the location of OCT scans in untreated and treated regions shown below. (*B*) ONL fraction at 34 wk as a function of vector titer injected at 24 wk. Data from treated (Tx, green) and untreated (UnTx, red) regions are contrasted. Dashed lines show the range of ONL fraction expected in untreated WT eyes.

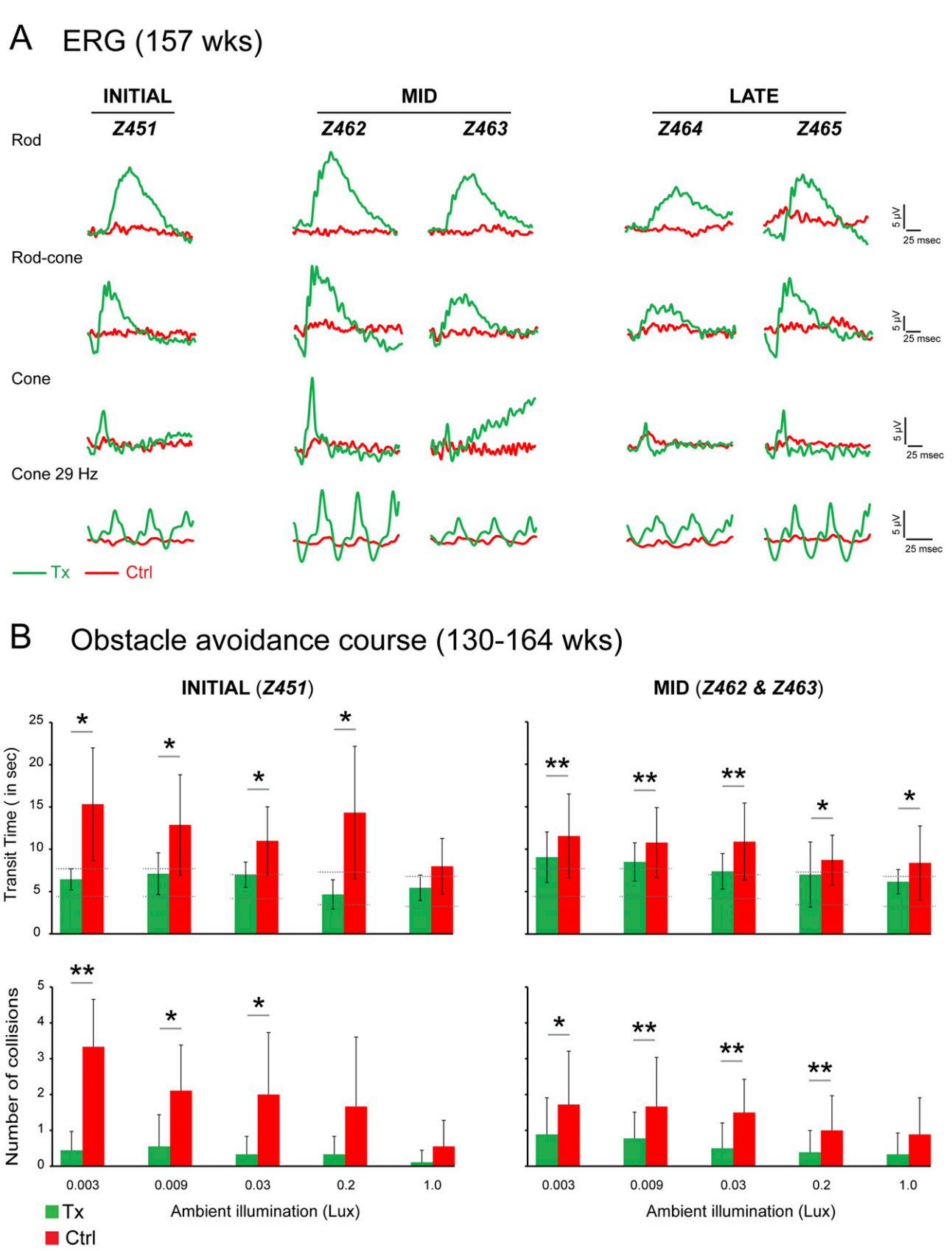

Fig. S3. Long-term rescue of photoreceptor function and visual behavior after gene therapy intervention at early, mid, and late stages of disease. (*A*) Representative ERG traces recorded at 157 wk of age in XLPRA2 dogs treated at 5 wk (Z451), 12 wk (Z462 & Z463) and 26 wk (Z464 & Z465) of age. (*B*) Mean (±SD) transit time and mean (±SD) number of collisions in an obstacle-avoidance course under different ambient light intensities. The treated vs.

Legend continued on following page

control eyes of one XLPRA2 dog (Z451) vector-injected at 5 wk of age and of two XLPRA2 dogs (Z462 & Z463) injected at 12 wk of age were compared after pooling data recorded during nine trials conducted between 130 and 164 wk of age. Gray dotted lines represent the 95% CI of the transit time of WT dogs ($n = 3$). No collisions were observed with these WT dogs. *$P < 0.05$, **$P < 0.001$ from generalized linear model testing between treated and control eyes.

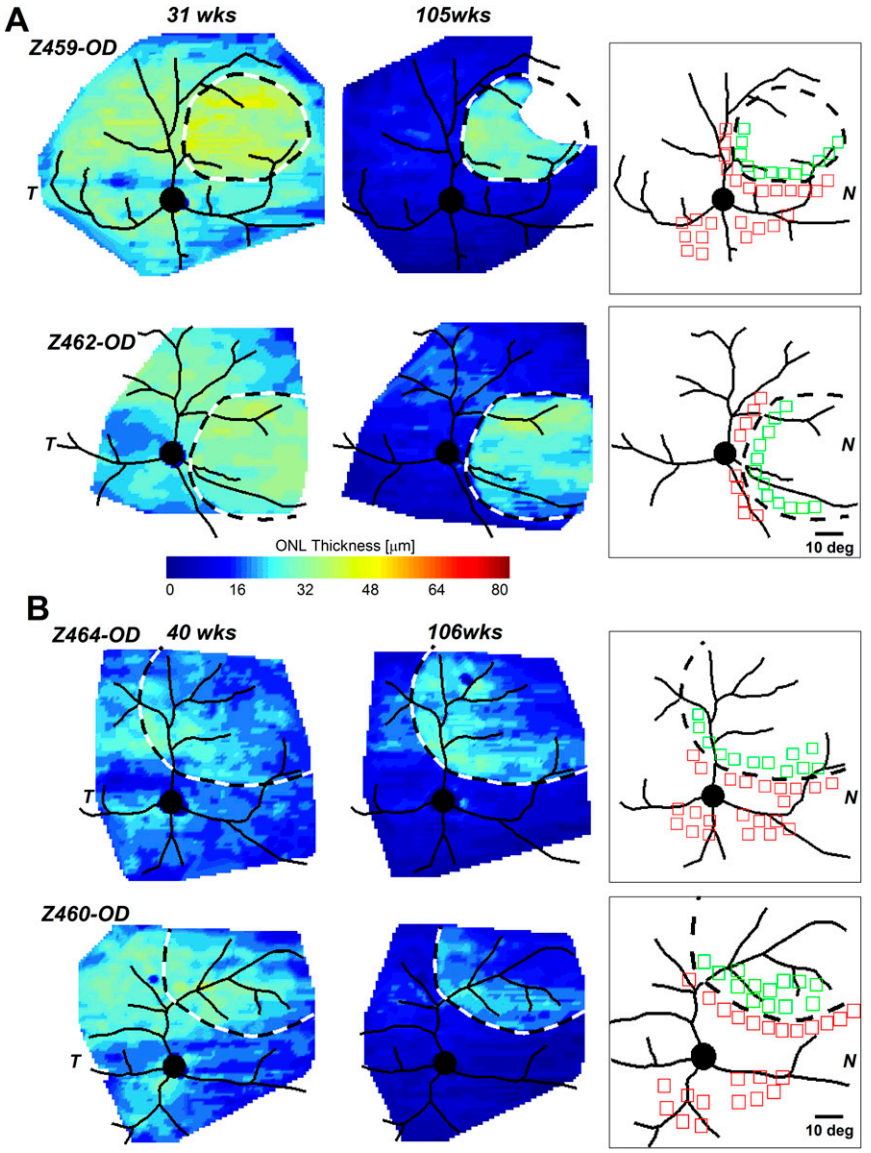

Fig. S4. Further examples of mid- and late-stage treatment. (*A*) Pseudocolor maps of ONL thickness topography at 31 and 105 wk of age in two XLPRA2 dogs treated at 12 wk of age. (*B*) Pseudocolor maps of ONL thickness topography at 40 and 106 wk of age in two XLPRA2 dogs treated at 26 wk of age. Dashed outline, the retinal region corresponding to the subretinal bleb. Schematic, right, paired loci across the treatment boundary and in the inferior retina chosen for quantitative evaluation (see Fig. 3*B* for plot of results that include these eyes). Eyes are shown as equivalent right eyes with optic nerve and major blood vessels overlaid for ease of comparability. T, temporal; N, nasal retina.

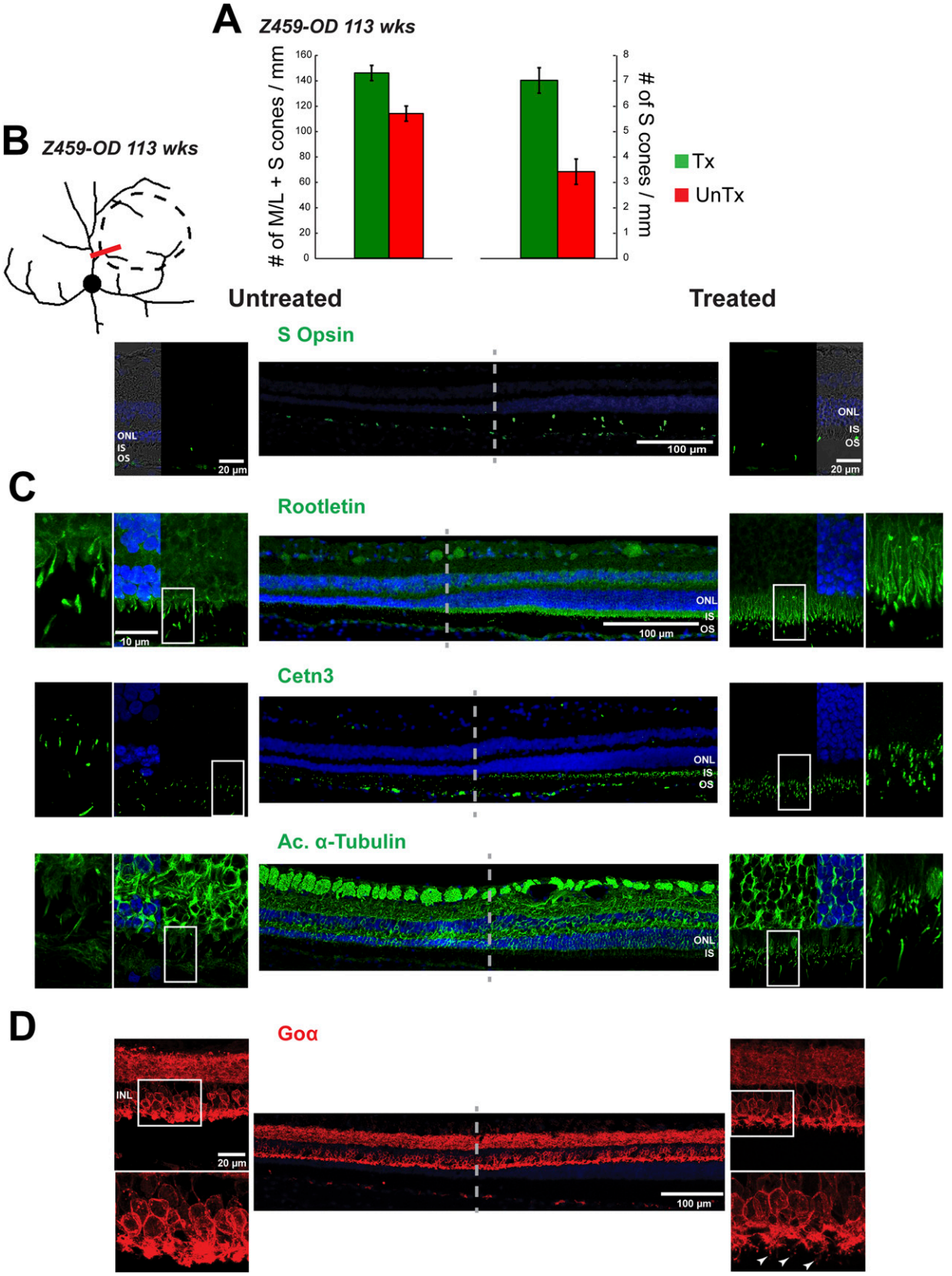

Fig. S5. Structural rescue of photoreceptors and bipolar cells in a XLPRA2 dog treated at mid-stage disease. Histology at 113 wk of age of dog Z459 injected at 12 wk. (*A*) Mean (±SD) number of (M/L + S) and S cones per millimeter of retina length in the treated and untreated areas ($n = 4$). (*B*) S cone opsin (green) IHC labeling in the untreated area (*Left*), across the treatment boundary (*Center*), and in the treated area (*Right*). The schematic drawing illustrates the treatment area (dashed black circle) and the location of the section showing the treatment boundary (red line). (*C*) IHC labeling of the sensory cilium of photoreceptors with rootletin, centrin-3 (Cetn3), and acetylated α-tubulin antibodies. (*D*) Goα IHC labeling of ON-bipolar cells. White arrows point to their dendrites.

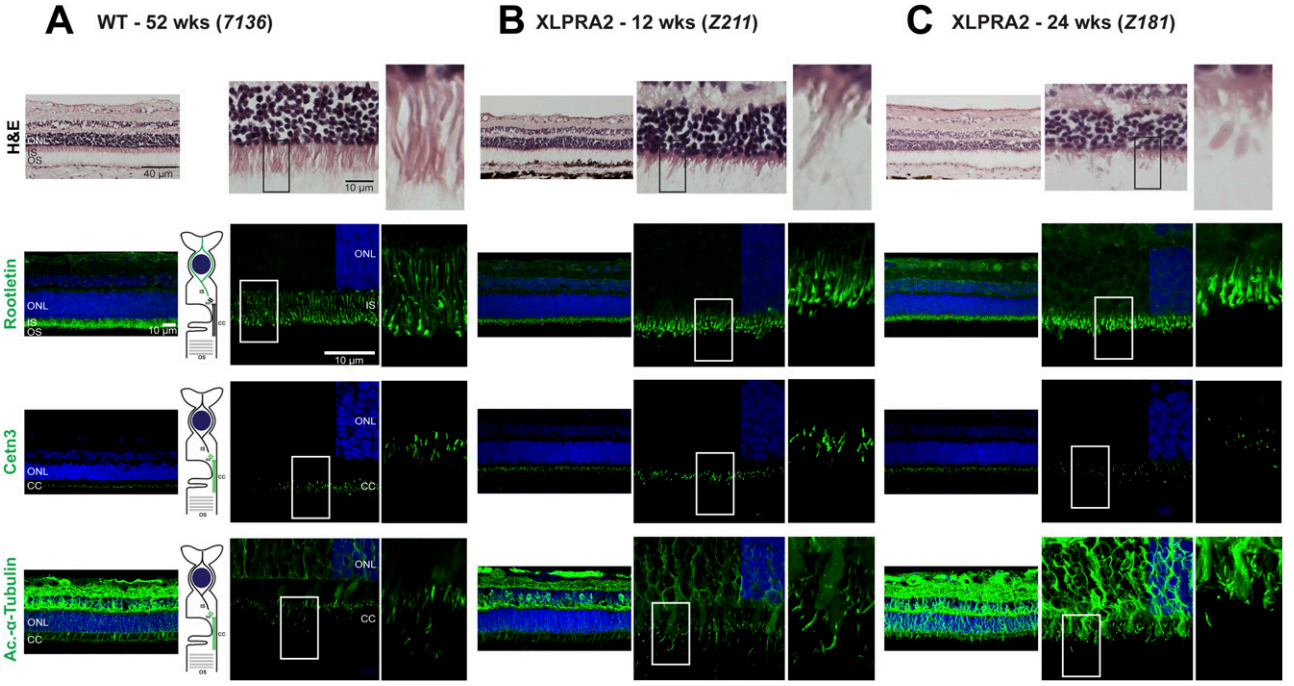

Fig. S6. Immunohistochemical labeling of the photoreceptor sensory cilium in WT and untreated XLPRA2 dogs at mid and late stages of disease. (*A*) Low and high magnification views of an adult WT canine retina labeled with H&E stain, rootletin, centrin-3 (cetn3), and acetylated α-tubulin antibodies. The schematics show the region of the photoreceptor sensory cilium labeled by these markers. (*B*) H&E and IHC labeling of an untreated XLPRA2 retina at mid-stage disease. (*C*) H&E and IHC labeling of an untreated XLPRA2 retina at late-stage disease.

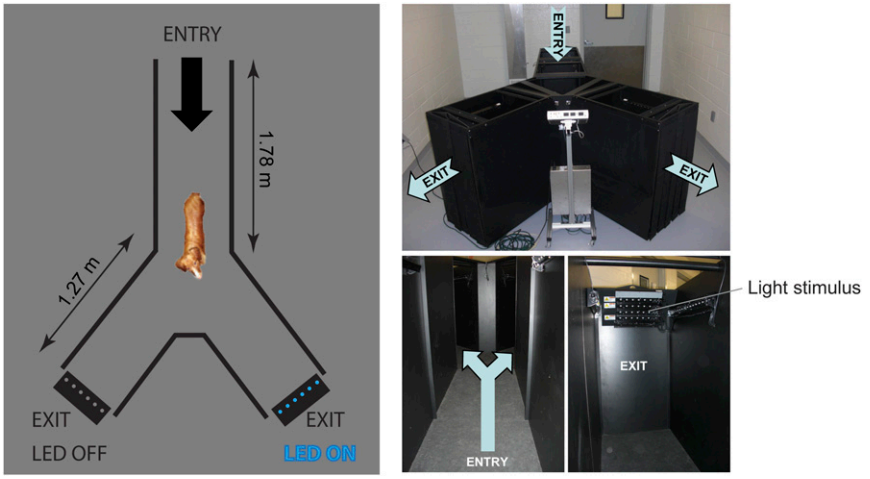

Fig. S7. Y maze apparatus for the testing of visually guided behavior in dogs. Plan (*Left*) and three photographs (*Right*) of the Y maze apparatus. (*Upper*) Overall view showing the central unit that controls the light stimuli at both exit arms. (*Lower Left*) View from the entry at dog's height. (*Lower Right*) View of the strip of LEDs located at the end of each exit arm. Note that the black cover that isolates the inside of the Y maze was removed on these photographs.

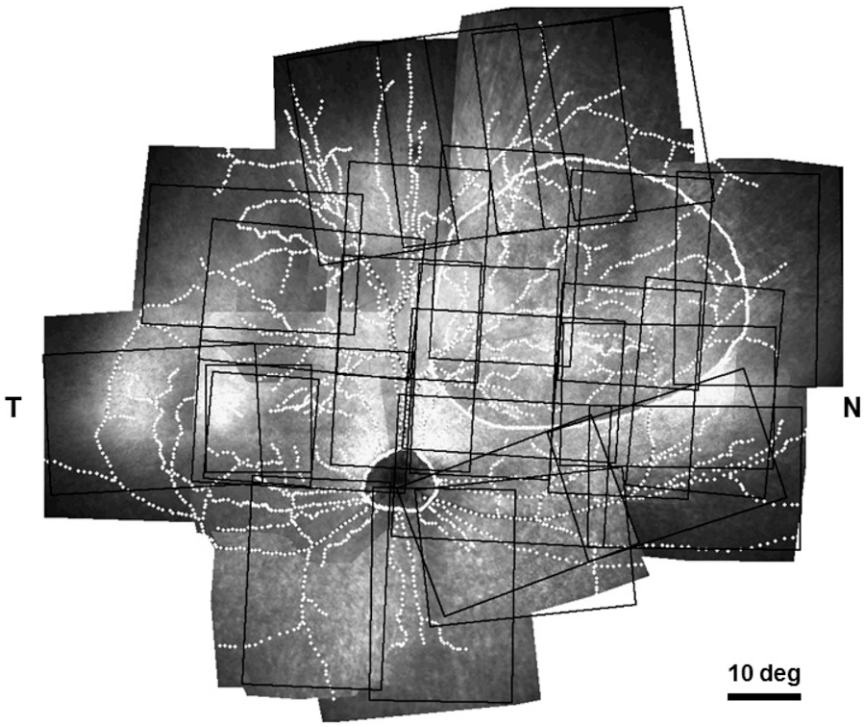

Fig. S8. Retina-wide topographic analysis. Cross-sectional OCT scans were performed in square or rectangular raster sets (black outlines) placed with overlap across vast regions of the retina. Postacquisition, wide angle image of retinal reflectance was produced (gray scale image), retinal blood vessels were traced (white dashed lines) and the optic nerve and bleb locations were overlaid (white lines). Using integrated OCT backscatter intensity, each raster scan set was placed across the retina by adjusting the location and rotation with respect to retinal features visible. T, temporal, N, nasal retina.

Table S1. Summary of the experimental procedures performed in the dogs of this study

		Age (wk)		Treatment				
Animal ID	Eye	Begin	End	Agent injected	Titer (vg/mL)/*volume (μL)*	Analysis	Studies	Figure
XLPRA2 dogs								
Z343	OD	8	/	/	/	OCT	Natural course of Dx	Fig. 2*D* Fig. S1 *C–E*
Z468	OD	5	38	AAV-hRPGR	0.05×10^{11}/*100*	OCT, ERG, Histology	Dose–response	Fig. 2*B*
Z468	OS	5	38	AAV-hRPGR	0.05×10^{11}/*70*	OCT, ERG, Histology	Dose–response	Fig. 2 *A–C*
Z467	OD	5	37	AAV-hRPGR	0.15×10^{11}/*70*	OCT, ERG, Histology	Dose–response	Fig. 2 *A–C*
Z467	OS	5	37	AAV-hRPGR	0.15×10^{11}/*140*	OCT, ERG, Histology	Dose–response	Fig. 2*B*
Z412*	OD	5	38	AAV-hRPGR	1.5×10^{11}/*70*	OCT	Dose–response	Fig. 2 *A–C*
Z412*	OS	5	38	BSS	*70*	OCT	Natural course of Dx	Fig. 2*D* Fig. S1 *D* and *E*
Z451	OD	5	Ongoing	AAV-hRPGR	1.5×10^{11}/*70*	OCT, ERG, Visual behavior, Histology	Dose–response	Fig. 2 *B* and *D* Fig. S3 *A* and *B*
Z451	OS	5	Ongoing	BSS	*70*	OCT, ERG, Visual behavior, Histology	Natural course of Dx	Fig. 2*D* Fig. S1 *C–E* Fig. S3 *A* and *B*
Z466	OD	5	40	AAV-hRPGR	15.1×10^{11}/*70*	OCT, ERG, Histology	Dose–response	Fig. 2*B*
Z466	OS	5	40	AAV-hRPGR	15.1×10^{11}/*70*	OCT, ERG, Histology	Dose–response	Fig. 2 *A–C*
Z459	OD	12	113	AAV-hRPGR	1.5×10^{11}/*150*	OCT, ERG, Histology	Natural course of Dx + Mid-stage Tx	Fig. 2*D* Fig. 3*B–G* Fig. S1 *D* and *E* Fig. S4*A* Fig. S5
Z459	OS	12	113	BSS	*150*	OCT, ERG, Histology	Natural course of Dx	Fig. 2*D* Fig. S1 *D* and *E*
Z462	OD	12	Ongoing	AAV-hRPGR	1.5×10^{11}/*150*	OCT, ERG, Visual behavior,	Natural course of Dx + Mid-stage Tx	Fig. 2*D* Fig. S1 *D* and *E* Fig. S3 *A* and *B* Fig. S4*A*
Z462	OS	12	Ongoing	BSS	*150*	OCT, ERG, Visual behavior	Natural course of Dx	Fig. 2*D* Fig. S1 *D* and *E* Fig. S3 *A* and *B*
Z463	OD	12	Ongoing	AAV-hRPGR	1.5×10^{11}/*150 (intravitr. control)*	OCT, ERG, Visual behavior	Natural course of Dx	Fig. 2*D* Fig. S1 *D* and *E* Fig. S3 *A* and *B*
Z463	OS	12	Ongoing	AAV-hRPGR	1.5×10^{11}/*150*	OCT, ERG, Visual behavior	Natural course of Dx + Mid-stage Tx	Fig. 2*D* Fig. S1 *D* and *E* Fig. S3 *A* and *B*

Table S1. Cont.

Animal ID	Eye	Age (wk) Begin	Age (wk) End	Treatment Agent injected	Treatment Titer (vg/mL)/*volume (μL)*	Analysis	Studies	Figure
Z460	OD	26	113	AAV-hRPGR	1.5×10^{11}/*150*	OCT, ERG, Histology	Natural course of Dx + Late-stage Tx	Fig. 2*D* Fig. 4 *B–G* Fig. 5 Fig. 6*B* Fig. S1*D* Fig. S4*B*
Z460	OS	26	113	BSS	*150*	OCT, ERG	Natural course of Dx	Fig. 2*D* Fig. 6*B* Fig. S1 *D* and *E*
Z464	OD	26	Ongoing	AAV-hRPGR	1.5×10^{11}/*150*	OCT, ERG, Visual behavior	Late-stage Tx	Fig. 6 *B–D* Fig. S3*A* Fig. S4*B*
Z464	OS	26	Ongoing	BSS	*150*	OCT, ERG, Visual behavior	Natural course of Dx	Fig. 2*D* Fig. 3*B* Fig. 4*B* Fig. 6 *B–D* Fig. S1 *D* and *E* Fig. S3*A*
Z465	OD	26	Ongoing	AAV-hRPGR	1.5×10^{11}/*150*	OCT, ERG, Visual behavior	Natural course of Dx+ Late-stage Tx	Fig. 2*D* Fig. 4 *A* and *B* Fig. 6 *A–D* Fig. S1 *C–E* Fig. S3*A*
Z465	OS	26	Ongoing	BSS	*150*	OCT, ERG, Visual behavior	Natural course of Dx	Fig. 2*D* Fig. 4*B* Fig. 6 *A–D* Fig. S1 *D* and *E* Fig. S3*A*
Z211†	OD	12	12	/	/	Histology	Natural course of Dx	Fig. S6
Z181†	OD	26	26	/	/	Histology	Natural course of Dx	Fig. S6
WT dogs								
EM249	OD	7	/	/	/	OCT	Control	Fig. S1 *B*, *D*, and *E*
AS340	OD	16	/	/	/	OCT	Control	Fig. S1 *B*, *D*, and *E*
D204	OD	22	/	/	/	OCT	Control	Fig. S1 *B*, *D*, and *E*
WBT60	OD	35	/	/	/	OCT	Control	Fig. S1 *B*, *D*, and *E*
D340	OD	43	/	/	/	OCT	Control	Fig. S1 *A*, *B*, *D*, and *E*
N284	OS	140	/	/	/	OCT	Control	Fig. S1 *D* and *E*
N269	OS	198	/	/	/	OCT	Control	Fig. S1 *D* and *E*
2133	OD	24	34	AAV-hRPGR	0.15×10^{11}/*150*	OCT	Dose determination	Fig. S2*B*
2133	OS	24	34	AAV-hRPGR	0.15×10^{11}/*150*	OCT	Dose determination	Fig. S2 *A* and *B*
2132	OD	24	34	AAV-hRPGR	1.5×10^{11}/*150*	OCT	Dose determination	Fig. S2 *A* and *B*

Table S1. Cont.

Animal ID	Eye	Age (wk) Begin	Age (wk) End	Treatment Agent injected	Treatment Titer (vg/mL)/*volume (μL)*	Analysis	Studies	Figure
2132	OS	24	34	AAV-hRPGR	1.5×10^{11}/*150*	OCT	Dose determination	Fig. S2*B*
2131	OD	24	34	AAV-hRPGR	15.1×10^{11}/*150*	OCT	Dose determination	Fig. S2*B*
2131	OS	24	34	AAV-hRPGR	15.1×10^{11}/*150*	OCT	Dose determination	Fig. S2 *A* and *B*
7136	OS	52	52	/	/	Histology	Control	Fig. S6
2211	OU	16	/	/	/	ERG	Control	/
N291	OU	27	/	/	/	ERG	Control	/
N290	OU	27	/	/	/	ERG	Control	/
GI115	OU	42	/	/	/	ERG	Control	/
GI114	OU	42	/	/	/	ERG	Control	/
D340	OU	105	/	/	/	ERG	Control	/
GI84	OU	184	/	/	/	ERG	Control	/

*Dogs were enrolled in a previous study (30).
†Dogs were enrolled in a previous study (29).

Table S2. List of primary antibodies tested and used in this study

Antigen	Host	Source; catalog no. or name	Working concentration
Human RPGR	Rabbit polyclonal	Sigma; HPA001593	1:100
Human cone arrestin	Rabbit	C. Craft, Univ. of Southern California; LUMIF	1:10,000
M/L cone opsin	Rabbit polyclonal	Millipore; AB5405	1:100
S cone opsin	Goat polyclonal	Santa Cruz Biotechnologies; SC-14363	1:50
Rod opsin	Mouse monoclonal	Millipore; MAB5316	1:200
Goα	Mouse monoclonal IgG1	Millipore; MAB3073	1:5,000
Glial fibrillary acid protein (GFAP)	Rabbit polyclonal	DakoCytomation; Z0334	1:1,000
Centrin3	Rabbit polyclonal	Uwe Wolfrum, Univ. of Mainz, Germany	1:400*
Acetylated α-Tubulin	Mouse monoclonal	Sigma; T7451	1:1,000*
Rootletin	Human monoclonal	AbD Serotec; HCA009	1:50*

*IHC protocol required heat-induced epitope retrieval.